LAPPEENRANTA UNIVERSITY OF TECHONOLOGY

LUT School of Energy Systems

Electrical Engineering

Industrial Electronics

Author of the thesis Dmitry Egorov

ANALYTIC EVALUATION OF THREE-PHASE SHORT CIRCUIT DEMAGNETIZATION AND HYSTERESIS LOSS RISK IN ROTOR-SURFACE-MAGNET PERMANENT-MAGNET SYNCHRONOUS MACHINES

Examiners: Professor Juha Pyrhönen

M. Sc. Nikita Uzhegov

ABSTRACT

Lappeenranta University of Technology
Faculty of Technology
Degree Program in Electrical Engineering

Dmitry Egorov

Analytic evaluation of three-phase short circuit demagnetization and hysteresis loss risk in rotor-surface magnet permanent magnet synchronous machines

2015

Master´s Thesis
84 pages, 37 figures, 2 tables, 1 appendix

Examiners: Professor Juha Pyrhönen
M. Sc. Nikita Uzhegov

Keywords: hysteresis loss risk, rotor-surface magnet PMSM, analytical calculation, permanent magnet, magnetic field distribution, stator current linkage, normal operational mode, symmetrical short circuit

Permanent magnet synchronous machines (PMSM) have become widely used in applications because of high efficiency compared to synchronous machines with exciting winding or to induction motors. This feature of PMSM is achieved through the using the permanent magnets (PM) as the main excitation source. The magnetic properties of the PM have significant influence on all the PMSM characteristics. Recent observations of the PM material properties when used in rotating machines revealed that in all PMSMs the magnets do not necessarily operate in the second quadrant of the demagnetization curve which makes the magnets prone to hysteresis losses. Moreover, still no good analytical approach has not been derived for the magnetic flux density distribution along the PM during the different short circuits faults.

The main task of this thesis is to derive simple analytical tool which can predict magnetic flux density distribution along the rotor-surface mounted PM in two cases: during normal operating mode and in the worst moment of time from the PM's point of view of the three phase symmetrical short circuit. The surface mounted PMSMs were selected because of their prevalence and relatively simple construction. The proposed model is based on the combination of two theories: the theory of the magnetic circuit and space vector theory.

The comparison of the results in case of the normal operating mode obtained from finite element software with the results calculated with the proposed model shows good accuracy of model in the parts of the PM which are most of all prone to hysteresis losses.

The comparison of the results for three phase symmetrical short circuit revealed significant inaccuracy of the proposed model compared with results from finite element software.

The analysis of the inaccuracy reasons was provided. The impact on the model of the Carter factor theory and assumption that air have permeability of the PM were analysed. The propositions for the further model development are presented.

ACKNOWLEDGEMENTS

This thesis was written in the Laboratory of the Electrical Engineering at Lappeenranta University of Technology at spring 2015.

I want to thank my supervisor Professor Juha Pyrhönen for such an interesting topic. This thesis helped me a lot to improve my knowledge of the field of the electrical machine design and gave many ideas for further development. I am really happy to provide the tool which makes the task of the machine design at least a little bit easier. I would like to thank my second supervisor M. Sc. Nikita Uzhegov for his help and fast response on the problems which occurred during the writing of the thesis work.

I would like to thank to my friends from Finland, Russia and Spain for priceless advices throughout my studies in Lappeenranta. I want to thank personally Emil Khaliullin for his wise advices, constant support and motivation during my studying at LUT.

Finally, I want to thank the most important people in my life: Galina Egorova, Nikolai Egorov, Alexander Egorov, Vladimir Bosomykin, Nadegda Bosomykina and Alexander Bosomykin for the constant support through all my life.

Dmitry Egorov

May 2015

Lappeenranta, Finland

TABLE OF CONTENTS

LIST OF SYMBOLS AND ABBREVIATIONS

Symbols

B	magnetic flux density scalar value, [Vs/m^2]
B_r	remanent flux density, [T]
b_d	tooth width, [m]
D	diameter, [m]
D_s	stator inner diameter, [m]
H	magnetic field strength scalar value, [A/m]
H_{cJ}	coercivity related to magnetization, [A/m]
H_{cB}	coercivity related to flux density, [A/m]
H_{PM}	field strength of the magnet, [A/m]
h_{PM}	height of permanent magnet, [m]
J	magnetic polarization
I_{DC}	direct current, [A]
i_d	*d*-axis component of current space vector in rotor fixed reference frame, [A]
i_q	*q*-axis component of current space vector in rotor fixed reference frame, [A]
i_x	x-component of current space vector in stator fixed reference frame, [A]
i_y	y-component of current space vector in stator fixed reference frame, [A]
k	iron magnetic resistance coefficient
k_{Cs}	Carter factor
k_{w1}	winding factor of current linkage fundamental
$k_{w\nu}$	winding factor of current linkage ν harmonic
L_d	synchronous inductance in *d*- axis, [H]
L_q	synchronous inductance in *q*- axis, [H]
m	number of phases
N	number of turns
p	number of pole pairs
Q	number of slots
R	stator resistance, [Ω]
S_δ	area of air gap, [m^2]
S_{PM}	area of permanent magnet, [m^2]

u_x x-component of voltage space vector in stator fixed reference frame, [V]

u_y y-component of voltage space vector in stator fixed reference frame, [V]

$W_{\tau p}$ winding pitch

α angle between permanent magnet flux vector and X-axis stator fixed reference frame, [rad]

β angle between stator flux vector and X-axis stator fixed reference frame, [rad]

δ_s load angle, [deg, rad]

δ_{es} equivalent air gap (slotting taken into account), [m]

Θ_1 current linkage of fundamental component, [A]

Θ_ν current linkage of the ν^{th} harmonic component, [A]

μ_r relative permeability

μ_0 permeability of vacuum, $4\pi \cdot 10^{-7}$ [Vs/Am, H/m]

σ ratio of the leakage flux to the main flux

τ_p pole pitch, [m]

τ_ν zone distribution

φ_s angle between stator voltage space vector and stator current space vector, [deg, rad]

ψ_{PM} permanent magnet flux space vector, [Vs]

ψ_x X-component of stator flux space vector in stator fixed reference frame, [Vs]

ψ_y Y-component of stator flux space vector in stator fixed reference frame, [Vs]

ω_R rotor electrical angular velocity, [rad/s]

Abbreviations

PMSM	Permanent Magnet Synchronous Machine
SM	Synchronous Machine
PM	Permanent Magnet
FEM	Finite Element Method
NdFeB	Neodymium Iron Boron, a rare earth magnet material
SSC	Symmetrical Short Circuit
RECo	Rare Earth Cobalt, a rare earth magnet material
AlNiCo	Aluminium Nickel Cobalt, magnet material
SCC	Short Circuit Currents

1 INTRODUCTION

The active development of the permanent magnets (PM) started in the beginning of the twentieth century. Later, in 1980's significant improvements of the PM magnetic properties allowed to design new practical type of the synchronous machine (SM) – permanent magnet synchronous machine. In this type of the synchronous machine the excitation winding is replaced by the PM material. This design solution helped to get rid of the excitation winding of the SM and brushes in the excitation system. Ability to obtain PMs with different shapes allows to design the magnetic circuit of the machine with the required no-load magnetic flux density. Further analysis revealed that replacing the exciting winding with the PM allows to increase the efficiency of the SM. A general assumption amongst designers was that there should be no losses in the magnets at all, which assumption has later been proven wrong.

Permanent magnet synchronous machines (PMSM) are become more popular nowadays. They are widely used in the industrial applications, e.g., wind power generators, traction motors, linear machines, high-speed machinery and in aerospace applications [1]. The main advantage of PMSM is higher efficiency compared to the Induction Machines (IM) and synchronous machines with exciting winding, which achieved by using the permanent magnets as a source of the excitation in the PMSM. This feature of PMSM allows, in principle, to get rid of Joule losses in the rotor which occurs during the excitation of SM with the excitation winding and thus increase the efficiency of the SM [2].

Permanent magnets are essential part of the PMSM and have strong influence on the machine's final properties. That is why it is very important to know and to predict possible problems which can take place during the operation of the PMSM. Traditionally, the risk of demagnetization in elevated temperatures and demagnetization due to Joule losses are considered as the main problem during the operation of PMSMs. It also should be mentioned that high temperature or high current linkages can demagnetize PM without any other effects. These two phenomena can affect PM together or separately and each of these phenomena can cause irreversible demagnetization of the PM. Good analysis and modelling of the PM demagnetization was provided by Ruoho in [3]. Results from [3] show that PM cannot be considered as the object with linear properties. The properties of

a PM are highly dependent on the temperature and the value of the external field strength [3], and these properties can be considered as linear only at certain operation area of the magnet.

PMs are conductive materials and significant Joule losses due to eddy-currents can take place in the PMs even during normal operation. These Joule losses in PMs are called eddy-current losses because the main reason for these losses are eddy-currents [2]. Prediction and calculation of the losses due to eddy-currents in PMs is not a straightforward task. Analysis of the literature shows that the eddy-current losses are mostly calculated with finite element method (FEM) based programs. Possible approaches for the analytical calculation of the eddy-current losses can be found in [2], [4] and [5].

Analysis of the literature [1] - [6] detects new possible source of the losses in PMs. This source of losses is hysteresis. Pyrhönen *et al.* in [1] suggest possible mechanism for the hysteresis losses and the explanation is mainly based on the non-ideality of the PM material structure. Hysteresis losses can take place even during the normal operation if the machine has not been correctly designed. This source of losses is not described accurately and measurement results provided in [1] did not estimate the amount of this type of losses. Authors in [1] claim that this type of losses cannot take place if the machine is skilfully designed. Literature analysis [1] shows that these losses can be easily prevented during the design process if the magnetic flux density in the PM during the operation will always remain lower than the remanent flux density of the material. This thesis studies if this condition can be estimated analytically.

External short circuit is another problem in PMSMs. Naturally short circuit occurrence varies largely in different machines and it is not even always necessary to design machines so that they are short-circuit tolerant. However, in many cases the machine must be short-circuit tolerant and therefore there should be reliable tools to analyse this phenomenon in the design phase. For example, a direct on line permanent magnet synchronous generator has to face short circuits every now and then because of different faults in the network supplied. Customers regularly want to be present during laboratory tests where the machine is shorted under its normal rated operation. Some other applications are such that no risk of demagnetization is accepted as the maintenance work

should be too expensive. As an example a wind turbine generator might be mentioned. There may also exist applications where replacing a faulty machine is finally cheaper than making sure that demagnetization will not take place during any fault.

During a short circuit the phase currents in the stator winding can have very high values. These currents can create external magnetic field strength which can partly or totally demagnetize the PM material in the PMSM. Tang *et al.* in [7] show that the PM operating point can have quite low values of magnetic flux density even during the direct-on-line starting. The short circuit in PMSM is a very chaotic process and depends on many factors: type of the short circuit, operating point of the machine, place where short circuit takes place, and parameters of the machine [8]. Literature review shows that FEM simulations are used to predict the possible problems with PM during the different short circuit faults. No simple analytical approach has been derived for the PM magnetic flux density distribution during the short circuit faults.

The above information shows that an analytical approach should be derived for the PM magnetic flux density distribution in the PMSM machine during the various operation modes. This approach should be based on the parameters of the PMSM which were obtained during the design process.

1.1 Aim of the work

The objective of this work is to predict possible hysteresis loss risks which can take place even during the normal operation mode of the PMSM and possible demagnetization of PM which can take place during a short circuit. The goal is to develop a simple tool which will show an approximate PM magnetic flux density distribution during the normal operation mode and the worst case of the three-phase short circuit. This tool should use only the parameters of the machine that have been obtained during the design process and should not be based on a finite element method software. The designer of an electrical machine can use the proposed solution for a fast and quite accurate estimation of the possible risk of the hysteresis losses and the magnet demagnetization. Naturally, it is wise to check the results by a FEM-based tool. However, bad designs can be rejected easily with this tool to speed up the design process significantly

1.2 Scientific contribution

New analytic models to analyse the demagnetization risk during a short circuit and the risk of hysteresis loss under normal operation are developed. The space vector theory is widely used in the modelling of rotating field machines. The theory of the magnetic circuits allows to analyse magnetic circuit on the stage of the preliminary design. These two theories are well known and provide good results comparing with FEM programs for the simple magnetic circuits. The proposed model is based on the combination of these two theories. The rotor-surface magnet synchronous machine is selected for analysis because of its prevalence and relatively simple construction of the rotor compared with other types of the rotor which are used in present-day PMSMs. The contribution of this work is to provide the simple analytical approach for the magnetic flux density distribution in PM of the rotor-surface magnet PMSM during the various operation modes. The tool derived can easily predict any possible problems in the PMs concerning hysteresis loss risk and partial demagnetization during a three-phase short circuit at the stage of the preliminary design.

1.3 Structure of the work

This thesis has the following structure:

- Chapter 1 presents the problem which will be observed in the thesis and shows the scientific contribution of the work. The theory about permanent magnets which are used in today's PMSMs is presented. The main characteristics and properties of the PMs are described. The theory concerning eddy-current losses and hysteresis losses, the winding theory, the theory of the three-phase short circuit analysis in the PMSM are presented in this chapter. The provided theory is used in the proposed solution.
- Chapter 2 is dedicated to the research theoretical development. The principles and assumptions used in the proposed solution are described here.
- Chapter 3 contains the application of the theory. The equations that are used in the proposed model are described in this chapter.
- Chapter 4 presents the verification of the theory. The comparison of the results obtained with proposed model and with FEM program is presented in this chapter.
- Chapter 5 presents conclusion and propositions for the further work

1.4 Permanent Magnets in Synchronous Machines

Permanent magnets (PM) differ from soft magnetic materials because of their ability to maintain remanent magnetization for a long time. Displacement of Bloch walls and Weiss domains is made deliberately difficult in hard magnetic materials. Material becomes magnetized when Weiss domains are aligned in parallel by high external field strength. The fine structure of material prevents displacement of Bloch walls. [2]

Even though permanent magnetism has been known for millennia the real industrial development of the permanent magnets started in the beginning of twentieth century. The main problems related to using permanent magnets are traditionally considered to be: 1) high risk of demagnetization due to the influencing of an external demagnetizing field or a temperature rise, 2) high price and 3) low energy product. Significant improvement in the performances of the permanent magnets was made with discovering AlNiCo materials in 1930s, ferrites in 1950s and rare-earth metals and cobalt compounds in 1960s. Nowadays polymer-bonded permanent magnets can be considered as the fastest developing field. [2]

According to Pyrhönen *et al.* [2], these are the most wide spread commercial magnetic materials for the rotating machines that have been used and are used:

1) AlNiCo magnets (iron and several other metals such as aluminium, nickel and cobalt metallic compounds). These materials have been in use because of their performances such as high remanence and operating temperatures, good temperature stability and corrosion resistance. This material, however has weak demagnetization properties and is rarely used nowadays in motor applications; [3]
2) Ferrite magnets are made of sintered oxides, barium and strontium hexa-ferrite. The features of ferrites are low cost, low remanence. Some ferrites do not conduct electricity. This can be very important in some applications; [3]
3) RECo magnets (magnets from rare-earth cobalt). These magnets have high remanence, high corrosion resistance, and relatively high maximum operating temperatures, but they are expensive due to the high price of cobalt [3]. The magnets have relatively high conductivity and are, therefore prone to eddy current losses. Also hysteresis losses are possible [2];

4) Neodymium magnets are neodymium–iron–boron magnets, produced with using the powder metallurgy technique. Also these magnets have relatively high conductivity and are, prone to eddy current losses. Also hysteresis losses are possible. [2]

1.4.1 Neodymium-Iron-Boron-Magnets

NdFeB magnets are used in the analysis of this paper, and their properties are described further. NdFeB magnets are mainly manufactured by sintering and consist of rare-earth metals (30-32 % of weight), about 1% of boron, and the presence of the cobalt is about 0-3%. The rest of the material is iron which, actually donates the magnetic properties for the material. The rest of the materials are just needed to maintain the orientation of iron grains in the material. The properties of the magnets depend on the magnet alloy and pressing methods (orientation). Generally Neodymium magnets' properties are highly depend on temperature, and the coercive force of the magnet is inversely dependent on the temperature. Oxygen and moisture can cause corrosion of magnets that means quite poor chemical resistance properties. Mechanical properties are poor, but permanent magnets usually are not considered as the machine constructional part [2]. Table 1 was adopted from [2] and presents the characteristics of NdFeB magnets.

Table 1 Characteristics of Neodymium magnets

Composition	Nd, Dy, Fe, B, etc.
Production	Sintering
Energy product	199–310 kJ/m^3
Remanence	1.03–1.3 T
Intrinsic coercive force, H_{cJ}	875 kA/m to 1.99 MA/m
Relative permeability	1.05
Reversible temperature coefficient of remanence	−0.11 to −0.13%/K
Reversible temperature coefficient of coercive H_{cJ}	−0.55 to −0.65%/K
Curie temperature	320 °C
Density	7300–7500 kg/m^3
Coefficient of thermal expansion in magnetizing direction	5.2 ×10^{-6}/K
Coefficient of thermal expansion normal to magnetizing direction	−0.8 ×10^{-6}/K
Bending strength	250 N/mm^2
Compression strength	1100 N/mm^2
Tensile strength	75 N/mm^2
Vickers hardness	550–650
Resistivity	110–170 ×10^{-8}Ωm
Conductivity	0–900 000 S/m

1.4.2 Main characteristics of the permanent magnets

Permanent magnet can be described by following characteristics:

1) remanent flux density B_r;
2) coercivity H_{cJ} (or H_{cB});
3) the second quarter of the hysteresis loop;
4) energy product $(BH)_{PMmax}$;
5) temperature coefficients of B_r and H_{cJ}, reversible and irreversible portions separated;
6) resistivity ρ;
7) mechanical characteristics;
8) chemical characteristics. [2]

It is desirable for a permanent magnet material to have a high value for saturation polarization, Curie temperature and anisotropy. The geometry of a machine should be implemented, in principle, in a way to get the maximum energy product from the permanent magnet [2]. In case of linear demagnetization curve the maximum energy product is found at $B_r/2$. However, often as high torque density as possible is wanted, and therefore, more permanent magnet material is used to get as high air gap flux density as possible. Thick magnets are used to get closer to the remanent flux density of the material. A magnet manufacturer usually gives only the second quadrant of the hysteresis loop for a permanent magnet material. Typical hysteresis loop presented in Fig.1 was taken from [3] for NdFeB magnet Neorem 453a.The dependence of the polarization J and the magnet flux density B can be written as [2]:

$$J = B - \mu_0 H. \tag{1}$$

Equation (1) shows that the demagnetization curves in Fig.1 are enough for the description of the permanent magnet characteristics. Generally, curves in Fig. 1 depict a typical hysteresis curve of neodymium magnet for the flux density and polarization [2].

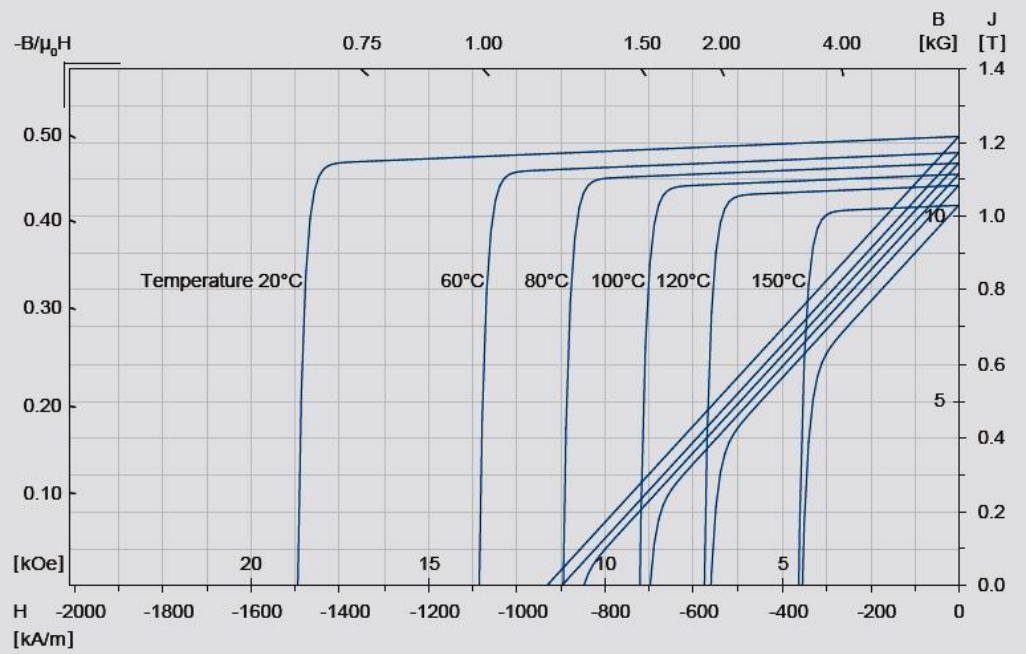

Fig. 1 Typical demagnetization curve $B(H)$ and polarization $J(H)$ at different operating temperatures for Neorem 453a. Modified from [9]

1.4.3 Operating point of a Permanent Magnet

As it was shown earlier in Fig. 1, usually permanent magnet material properties are described by the hysteresis curves which normally are given only for the second quadrant of the hysteresis loop. Magnetic properties of the PM are highly dependent on the temperature, and this is why the hysteresis curves are given for the different temperatures. Manufacturer gives two types of curves: *BH*-curves, which show the flux density of the magnet as a function which depends on the magnetic field strength, and *JH*-curves, which show the magnetic material polarization as a function of the magnetic field strength. Each point on a *JH*-curve is related to a corresponding point of the *BH*-curve and this relation described by [3]

$$B_m = \mu_0 H_m + J_m. \tag{2}$$

The operating point of the permanent magnet can be found by using the hysteresis curves given by the manufacturer. The external demagnetizing magnetic field strength affecting the permanent magnet (H_{PM}), based on solving of the magnetic circuit, can give the flux density of PM according to the hysteresis curves and the temperature of the magnet.

1.4.4 Demagnetization of Permanent Magnets

Demagnetization of permanent magnets can take place in rotating machines. Fig. 2 shows the effect of the demagnetized magnet behaviour.

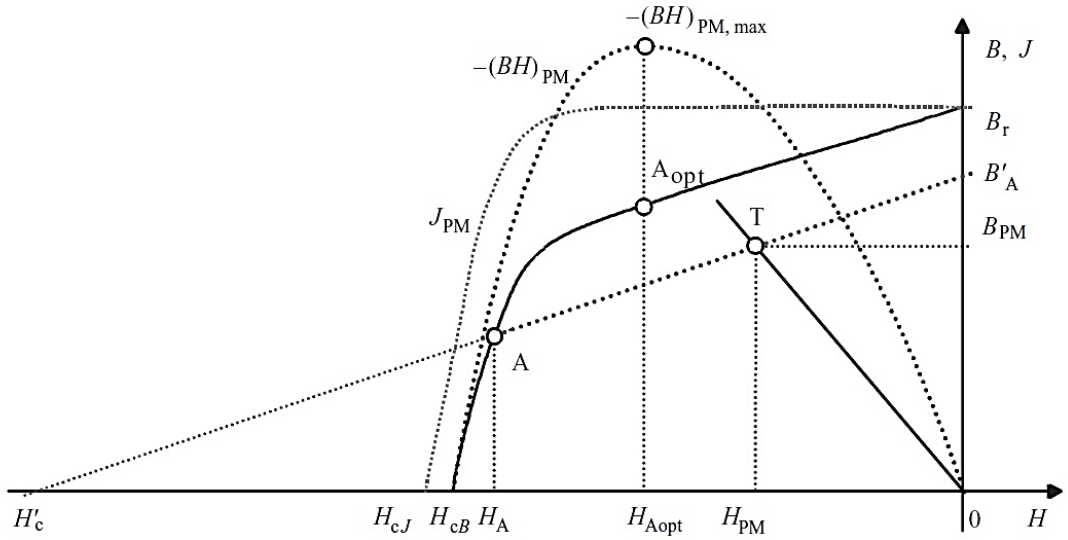

Fig.2 The effect of demagnetization on the magnet behaviour. Modified from Design of Rotating Electrical Machines [2]

In Fig. 2 it can be concluded that if the magnet operating point falls down to the non-linear part of the magnetization curve (e.g. point A in Fig. 2), the magnet is partly demagnetized, its remanent flux density becomes lower and the magnetization curve changes (now it becomes H_c`$-$ $B$`$_A$). If the operating point stays clearly in the linear region, there is no risk of demagnetization [3]. In [2], the possible situations that can cause the demagnetization are described as follows:

1) increasing of a temperature due to the machine's overload or infringement of normal cooling
2) short-circuit at the terminals of the machine
3) direct-on-line starting

According to [3] it is not possible to detect clearly whether demagnetization was caused by a too high temperature or by too-high current. Fig. 3 taken from [2] shows the recoil behaviour of a NdFeB magnet due to partial demagnetization.

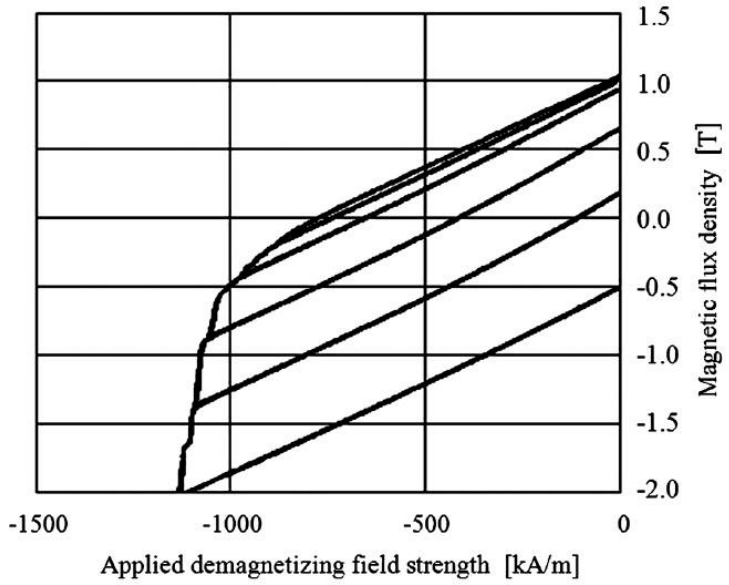

Fig.3 Recoil behaviour of NdFeB magnet sample. Modified from from [1]

If the operating point will be lower than the part where the operating line becomes non-linear, then partial demagnetization occurs. The remanent flux density is reduced in the demagnetization. A new line, which is called the recoil line, can be drawn from the lowest working point. It is stated in [3] that the slope of the recoil line can be considered approximately linear in case if the demagnetization is less than 10%. If the permanent magnet is highly demagnetized, the recoil line will be slightly bent upwards because of the magnetic domain structure. After the demagnetization has occurred, the recoil line must be used instead of the original *BH*-curve of the saturated magnet in the working point analysis [3].

Next, possible situations mentioned above are considered in more details. The main reason which can cause irreversible demagnetization is the high external field strength and the permanent magnet temperature increase [2]. Short-circuit can cause both of these conditions. Short-circuit first causes a high current transient and then the temperature is increasing due to the significant increase of Joule losses [3]. According to Ruoho [3] the most dangerous short-circuit is a phase-to-phase short-circuit, and its negative effects depend on the configuration of the network and a situation in which this short-circuit occurred. Symmetrical three phase short-circuit is considered slightly less risky.

Irreversible demagnetization of the permanent magnets can take place if the machine is overheated. Possible situation for this can be loss of cooling, dirty cooling channels, high

ambient temperature or selecting electrical machine with inappropriate duty-cycle [3]. Eddy-current losses is another factor influencing additional heating of the permanent magnets. Eddy-currents are quite difficult to model analytically. Mostly Eddy current losses are modelled by using Finite Element Method (FEM) Programs, but good analytical approach can be taken from [2]. If there is a big error in the prediction of eddy-current losses than the machine will be overheating on the nominal load and a risk of the demagnetization of permanent magnets increase accordingly [3].

In [1] the hysteresis losses are described. These losses can be a reason for the extra heating of the permanent magnet material in certain operational conditions. According to [2] these hysteresis losses do not occur in a normal operation of synchronous machines and eddy-current losses should be considered the major losses in the permanent magnets during the normal operation. However, it is shown in [1] that certain wrongly designed machine configurations the hysteresis losses are also possible at the normal operational point. The mechanism of hysteresis losses will be observed later.

Partial demagnetization of the permanent magnets can take place during the line start of PMSM. Such a machine is connected directly to a supplying network without frequency converter. The cage winding accelerates the rotor of a permanent synchronous machine till it synchronizes with the stator field [3]. Good simulation of a PMSM direct-on-line start was provided in [7]. Tang *et al.* in [7] provide the simulation of the permanent magnet average operating point. It can be concluded from [7] that the PM average operating point fluctuates significantly during the direct-on-line start. Average magnetic flux density of PM can be even 80% lower than its nominal value according to simulation results from [7]. If the lowest point lies below the linear part of the operating curve, permanent magnet partial demagnetization can take place.

Next, the effect of armature reaction on permanent magnet should be observed. Armature reaction takes place in all rotating field machines and its influence results in distortion of the resulting magnetic field of the electrical machine. Permanent magnets have to tolerate this influence. When the development of permanent magnets was in its infancy the permanent magnets could not tolerate even a little demagnetizing armature reaction. Present day magnets can, however, fairy well tolerate demagnetizing armature reaction

[2]. The mechanism with which the armature reaction influences on the working line of magnet depicted in Fig. 4 and Eq. (2) [2].

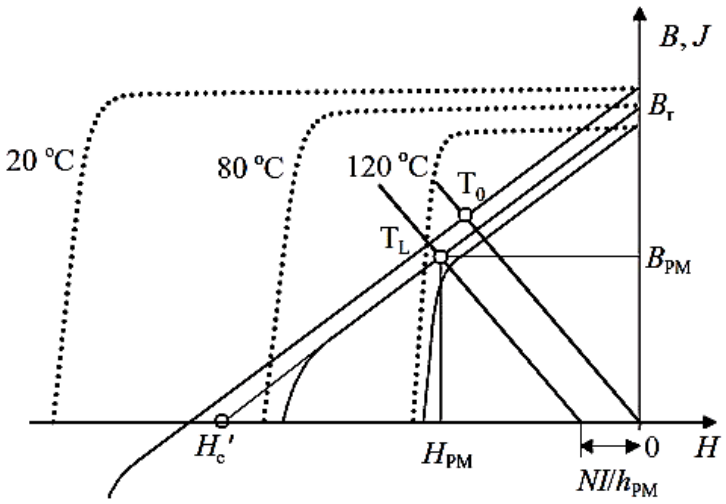

Fig. 4 Effect of armature reaction on the magnet's working line. Modified from Design of Rotating Electrical Machines [2]

Fig. 4 shows the effect of an armature reaction with negative sign on the permanent magnet working line behaviour. The operating point T_0 corresponds to the no-load operation at 20°C. At load with demagnetization current I the operating point is T_L. The operating temperature is increased to 80°C and the working line is shifted at the value of NI/h_{PM}. According to Fig. 4 if temperature is increased to 120°C with the same demagnetizing current, the operating point T_L can be located below the linear part of the *BH*-curve and it can lead to the partial demagnetization of the permanent magnet. It is stated in [2] that there is the following relation between the flux density of a permanent magnet and the armature reaction current:

$$B_{PM} = -(1+\sigma)\mu_0 \frac{h_{PM} S_\delta}{\delta S_{PM}} \left(H_{PM} + \frac{NI_{DC}}{h_{PM}} \right). \quad (3)$$

Eq. 3 and Fig. 4 show significant influence of the armature reaction on a permanent magnet behaviour.

In this paragraph typical situations, which can cause demagnetization, have been considered. It is very important to mention that the magnets are not demagnetized equally in rotating electrical machines. As an example it is stated in [1] that in case of a

synchronous generator with rotor-surface mounted magnets the PM front edge is demagnetized first due to the high armature reaction.

1.5 Losses in Permanent Magnets

1.5.1 Eddy current losses

Eddy-current losses are considered as the dominant losses in the permanent magnets of PM machines. These losses can result in a thermal demagnetization of the magnet if the machine is not correctly designed [2]. It is difficult to determine the eddy-current losses analytically and in most cases FEM programs are used for that. Generally, Maxwell's equations with quasistatic approximation are used for modelling [2].

Next, some theory for possible eddy-current losses is presented. In rotating field machines most of the parts are experiencing an alternating flux. If we consider a PMSM, a rotor surface can experience high-frequency components of the flux density which occur due to changes of permeance as a result of the stator slotting. In case of solid rotor of a synchronous machine the harmonic losses mostly occur at the surface of the rotor. The amplitudes of these harmonics are low because of a large air gap, but cannot be neglected [2]. Voltages are induced in the conductive material due to the alternating flux influence. These induced voltages result in eddy currents in material, which tend to resist changes of the flux. [1]

Negative effect from the eddy currents is mainly dependent on the material resistivity if machine is correctly designed. If the material has a high resistivity, eddy currents can be very small. For example, iron laminations are used for decreasing the negative effects from this phenomenon in electrical steels. Resistivity of the permanent magnets cannot be considered as very high. For NdFeB magnets the resistivity is about 110-170 $\times 10^{-8}$ Ωm. It is about 5-10-fold compared to the resistivity of steel. PM are usually mounted on the surface of the rotor and that makes them prone to permeance changing-caused harmonics, current linkage harmonics and time harmonics. This means that eddy current losses occurred in permanent magnet machines and this phenomenon cannot be neglected. It is also impossible to avoid it by machine design because of low conductivity of PM. Main contributors to creating this type of losses are slot harmonics and frequency switching harmonics, but according to Pyrhönen *et al.* [2] slot harmonics in low-speed

machines with semi-closed slots may be small [2]. Good analytical calculation of Eddy current losses in PMSM is provided in [2].

1.5.2 Hysteresis losses

Hysteresis losses in permanent magnet material should be considered besides the Eddy current losses. According to Pyrhönen *et al.* [2] these losses do not take place during normal operation of electrical machines. Machine has to be designed so, that the operating point of the permanent magnet is as close as possible to the point with the maximum energy product. This practice helps minimizing the amount of PM material in PMSM and reduces costs. Authors in [1] claim that so-called hysteresis losses may be present in rotating field permanent synchronous machines. Further, the possible mechanism of creating hysteresis losses is observed. In theory, permanent magnet material should have constant polarization *J* which should not be dependent on the influence of external field strength *H*. Normally, external field strength *H* is always trying to demagnetize the permanent magnets. Such a behaviour leaves no space for hysteresis losses [1].

Polarization of magnet should be constant until the demagnetizing magnetic field strength reaches a very high level and PM loses its polarization partially of totally. Hysteresis loop similar to the soft magnetic materials can be present in PM if the magnetic field strength varies with extremely high amplitude and also changes its sign. Fig. 5 adopted from [1] shows the polarization behaviour in a PM due to varying extremely high magnetic field strength which changes its sign. *BH*-curve of the material is also illustrated. [1]

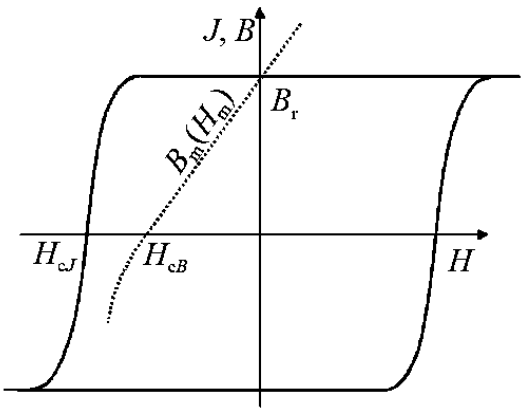

Fig. 5 Polarization behaviour in a PM due to affecting extremely high magnetic field strength which changes its sign. Modified from [1]

The demagnetization curve forms a straight line between the point of remanent flux density B_r and coercive force H_{cB} in ideal case. Authors in [1] state that when the polarization is constant, and the PM material has no soft phase its permeability equals to the permeability of vacuum μ_0 and the relative recoil permeability of PM material is μ_r = 1. But in real permanent magnets the recoil permeability is about μ_r = 1.04 and PM material shows some behaviour of a soft magnetic material [1]. Due to spin fluctuations or small nuclei of domains full saturation is practically impossible even after applying extremely high fields [10]. This phenomenon means that some soft phases in addition to the hard magnet phase can exist in permanent magnets and this can change the polarization of a magnet very little. This polarization changing can be the reason for some hysteresis losses in a permanent magnet. Fig. 6 and Eq. (4) taken from [1] show ideal and real behaviour of the permanent magnet polarization in the second quadrant according to the assumptions, described above.

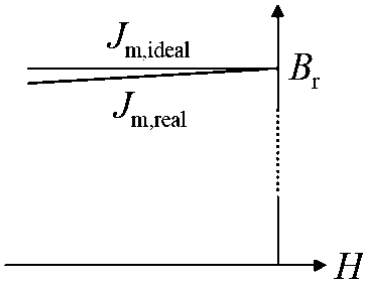

Fig. 6 Ideal and real behaviour of permanent magnet polarization in the second quadrant. Modified from [1]

$$J_m = B_r + \mu_0(\mu_r - 1)H_m \,. \tag{4}$$

Authors in [1] state that an additional flux density curve in the second quadrant of operation can be prone to hysteresis which depends on the recoil permeability, the history and the magnetic field strength. Possible hysteresis mechanism in sintered magnets can be described by representing the magnet as a theoretical alloy consisting of hard magnetic phase and little amount of soft magnetic phase. These two materials have remanent flux densities B_{r1} and B_{r2}, coercive forces H_{c1} and H_{c2}, respectively. Fig.7 taken from [1] shows the behaviour of such alloy with simplified hysteresis and saturation behaviour.

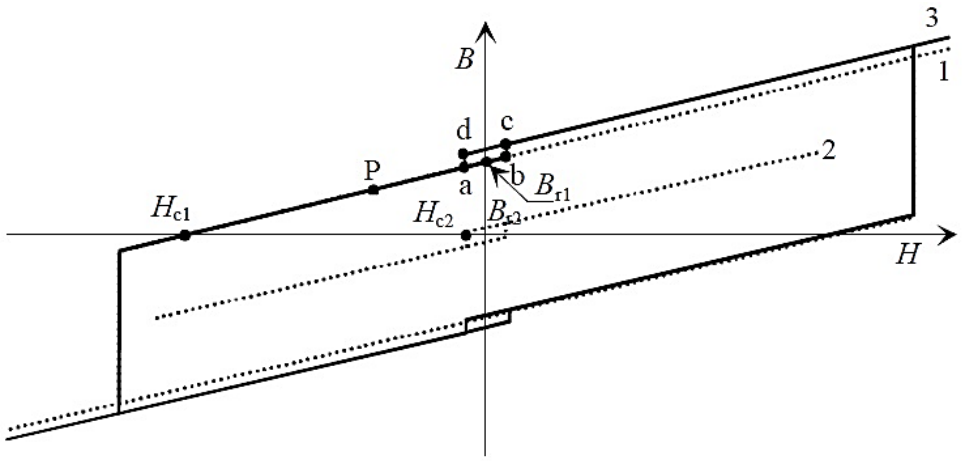

Fig.7 Behaviour of alloy with different remanent flux densities B_{r1} and B_{r2} and coercive forces H_{c1} and H_{c2}. Modified from [1]

Curve 1 represents totally polarized permanent magnet phase of the magnet. Curve 2 shows a material which can be considered as significantly softer material, because of low remanence and coercivity. This material can be used for describing the soft phases of a permanent magnet material, which are inside of totally polarized domains. Curve 3 depicts the behaviour of the permanent magnet according to the material behaviour simplifications. This curve was obtained by combining curves 1 and 2. Actually curve 3 depicts the behaviour of a sintered PM in a simplified way. The most interesting part of this curve is the resulting hysteresis loop a-b-c-d. Point P represents the normal working point of magnets in a permanent magnet synchronous machine.

Next, the behaviour of a permanent magnet with the influence of an external magnetic field strength is observed. When the armature reaction has positive sign and a very strong magnetic field strength, the operating point of the magnet can move towards point a, b or even c. With further increasing of positive field strength, the increasing of flux density will occur according to the permeability of the material. When the magnetic field strength *H* becomes smaller and goes negative, then the operating point moves through points c, d, a, and P. This behaviour can be used for describing possible mechanism of hysteresis losses in permanent magnets. [1]

Authors in [1] state that the hysteresis losses can occur in a permanent magnet machine even in normal operation mode if the armature reaction is exceptionally high. The field strength in permanent magnets varies very strongly and even the smallest hysteresis in permanent magnet material can result in noticeable hysteresis losses.

Hysteresis losses are difficult to measure. Certain measurements are described in [1]. As the result of measurements in [1] it can be said that the hysteresis losses are normally not present when a magnet operates in the second quadrant of the hysteresis loop and the presence of the hysteresis losses was not established with the measurements in [1] because of significant Eddy current presence and insufficient accuracy of the measurements. It is also shown in [6] that the hysteresis losses can be even higher than eddy current losses even at 50 Hz.

Influence of hysteresis losses in rotating field permanent magnet synchronous machines is observed further. Presence of air gap in this machines results in an apparent negative field strength affecting the magnet. This negative field strength moves the magnet operating point from B_r to lower flux densities. In conventional machines an armature reaction always exists when the machine operates under load. This armature reaction distorts the resulting magnetic field of the air gap and magnet respectively. Armature reaction causes different operating points at different parts of a magnet, so the magnet cannot be characterized by its average operation point. [1] Authors in [1] claim that due to the always opened air gap in rotating field machine and magnetic voltage drop in the air gap the operating point of the magnet should not exceed the remanent flux density B_r. Slightly demagnetizing stator current makes the operating point of permanent magnet even lower. This is a guarantee that the magnetic field strength never goes positive.[1] But authors in [1] also state that in some situations it can be necessary to select the operating point of magnet very close to B_r, even about $0.8 – 0.9\ B_r$ at no load. In that case due to strong armature reaction some parts of PM can operate at flux densities higher than B_r and these parts of the permanent magnets are obliviously prone to hysteresis losses. According to the results of FEM simulations of the permanent synchronous machine with strong armature reaction in [1], the magnetic flux densities of the leftmost and rightmost part of the magnet can significantly differ from average permanent magnet operating point. This makes part of magnet operating with higher flux density be prone to hysteresis losses.

Analysis of permanent magnet hysteresis losses in [1] shows that in a carefully designed machine they are much less than the Eddy current losses because all parts of the permanent magnet operate in the second quadrant of the *BH*-curve and do not go above B_r. However, during a high accelerating torque for example in traction drives or due to a

strong armature reaction parts of the magnets can operate above B_r and hysteresis behaviour of the permanent magnet can take place. Armature reaction estimation requires the analysis of the magnetic field distribution in the machine during its design process, and if the risk of hysteresis losses is present, the machine has to be redesigned.

1.6 Phase windings of electrical machines

In this paragraph basics of the rotating field windings are observed. Work principle of PMSM is based on the magnetic fields interactions of permanent magnet and field, produced by the stator winding. Stator winding of synchronous machine can be considered as an armature winding, because its task is to receive or deliver active power to the external system. Armature reaction of an armature winding is one of the inherent phenomena caused by this type of winding. The effect of armature reaction results in distortion of the air gap magnetic field caused by fields, induced by the armature currents. Ordinary, two types of stator windings are used in PMSM depending of relation between L_d and L_q inductances: [2]

1) if the number of slots per pole and phase $q > 0.5$, the winding is considered as distributed slot winding;
2) if $q \leq 0.5$, the winding is considered as winding with concentrated pole;

1.6.1 Poly-phase slot windings

Poly-phase AC windings are used for generation of the rotating field. Usually windings are three phase windings because of three phase supplying network, but generally any number of phases is possible. Basic values that describe symmetrical poly-phase winding are pole pitch τ_p, number of pole pairs p, diameter D, phase zone distribution τ_v, number of slots in each zone q, the stator number of slots Q. [2] Determination and meaning of listed parameters:

Pole pitch τ_p, [m] determines the arc that covers 180 electrical degrees and calculated as

$$\tau_p = \pi D/2p \ . \tag{4}$$

Phase zone distribution τ_v, [m] shows the proportion of each phase in the pole pitch and is determined as:

$$\tau_v = \tau_p / m \, . \tag{5}$$

Number of slots in each zone q determines the number of slots per pole and phase and is calculated as:

$$q = Q / 2pm \, . \tag{6}$$

If q is fractional, then this winding is a winding with the fractional slot.

Fig. 8 taken from [2] shows three-phase 4-pole integral slot winding with q = 1, Q = 12. From this figure it can be seen that U, V, W (which are called the phase zones) are located at equal distances on the stator of the machine. The windings in a three-phase system should be positioned with 120 electrical degrees shift from each other. In case, depicted in Fig. 9, winding consists of 360 mechanical degrees and 720 electrical degrees due to four poles in this case. This means that two positive zones are needed for each of three phases U, V, W and positive zones of each phase will be 60 mechanical degrees from other phases. Negative zone of each phase should be 180 electrical degrees from positive zone, in case of four pole machines 180 electrical degrees equal to 90 mechanical degrees. Fig. 8 shows winding, described above.

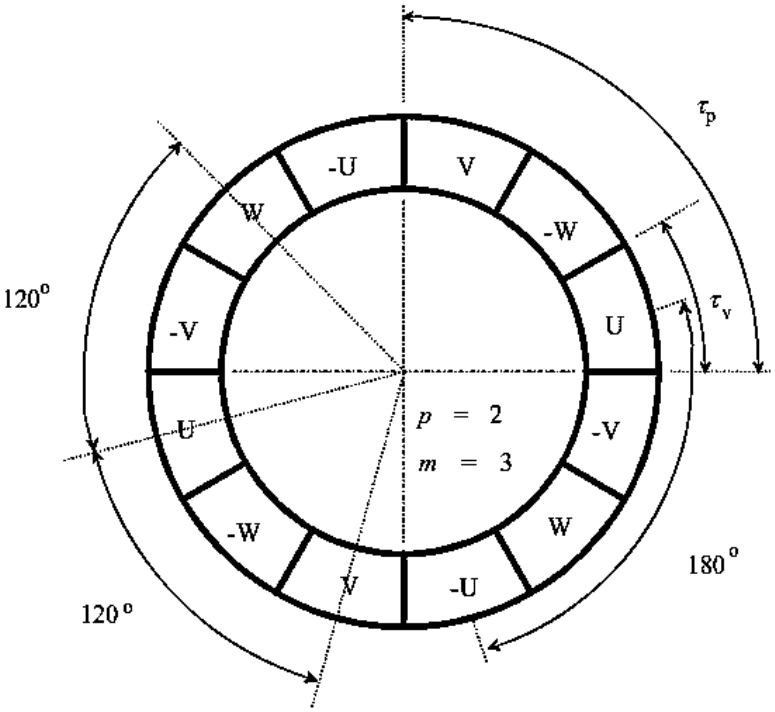

Fig. 8 Three-phase 4-pole integral slot winding with q = 1, Q = 12. Modified from Design of Rotating Electrical Machines [2]

1.6.2 Current linkage of three-phase Integral Slot Stator Winding

Stator three-phase integral slot winding with the number of phases m = 3, number of pole pairs p =1, number of slots per pole and phase q = 1, and number of stator slots Q = 6 can be considered as the simplest three-phase rotating field winding. Production of current linkage of the winding is studied further. Fig. 9 adopted from [2] shows location of conductors of each phase. In this case 1 mechanical degree is equal to 1 electrical degree because of p = 1. The polarity is depicted at the moment when the current in phase U has its maximum value and goes through in the first conductor.

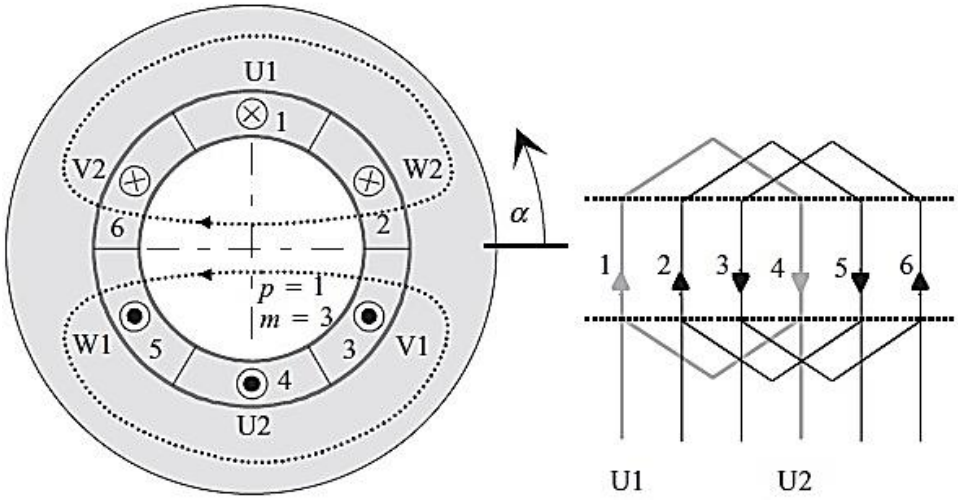

Fig. 9 Location of conductors of each phase in the three-phase integral slot winding with Q = 6, p = 1, m = 3 and q = 1 Modified from Design of Rotating Electrical Machines [2]

Fig. 10 and Fig. 11 taken from [2] show principles of the current linkage production and distribution in the three-phase integral slot winding with Q = 6, p = 1, m = 3 and q = 1. First, Fig. 10 shows the current linkage waveform and its fundamental harmonic when only the single phase U in the winding is fed by the current. The current linkage waveform is rectangular that actually means that it contains a huge number of low order harmonics.

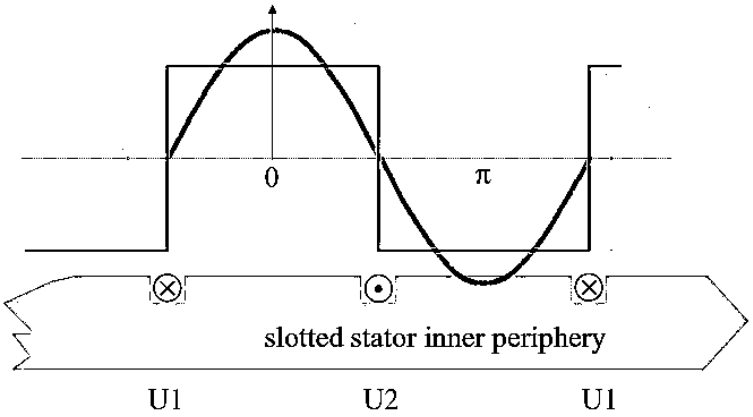

Fig. 10 Current linkage and its fundamental when only one phase U of the winding is fed by current. The current linkage waveform is rectangular and very far from sinusoidal Modified from Design of Rotating Electrical Machines [2]

In Fig. 11 all three phases are fed by currents and the current linkage distribution shown at moment t_1 and t_2. Waveforms of the current linkage are still far from sinusoidal but less distorted than in case described above for one phase.

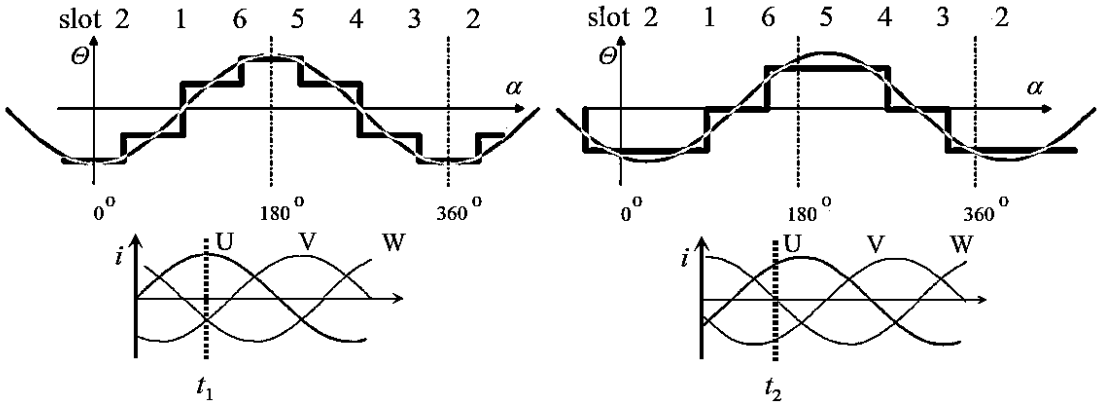

Fig. 11 Current linkage distribution at moment t_1 and t_2 for the three-phase integral slot winding with Q = 6, p = 1, m = 3 and q = 1 Modified from Design of Rotating Electrical Machines [2]

The current linkage at moment t_1 can be described in the following way. Observing starts from slot 2, which belongs to phase W and thus has current which flows from observer (depicted by the cross sign). This is depicted by increasing of current linkage (positive step) and value of this step depends on the current value in this phase at time t_1. The current linkage will be the same until slot 1. Slot 1 belongs to U phase and has current two times as big as the current of slot 1 and with the cross sign again, so current linkage step will be positive and twice bigger that step after slot 2. Then slot 6 causes a positive step with the value equal to the value of the step after slot 2. Slot 5 belongs to phase W, it has negative sign and current instantaneous value half of U, so it produces negative step

with the value equal to step after slot 5. The same principle is used for other slots and the resulting current linkage distribution is shown in Fig. 11. From this observation it can be concluded that the form of current linkage will be more sinusoidal if number of steps will be increased. Fig. 12 from [2] shows the same principle of drawing current linkage for winding with the following parameters: $Q = 12$, $m = 3$, $p = 1$ and $q = 2$ at the same moment of time as in Fig. 11.

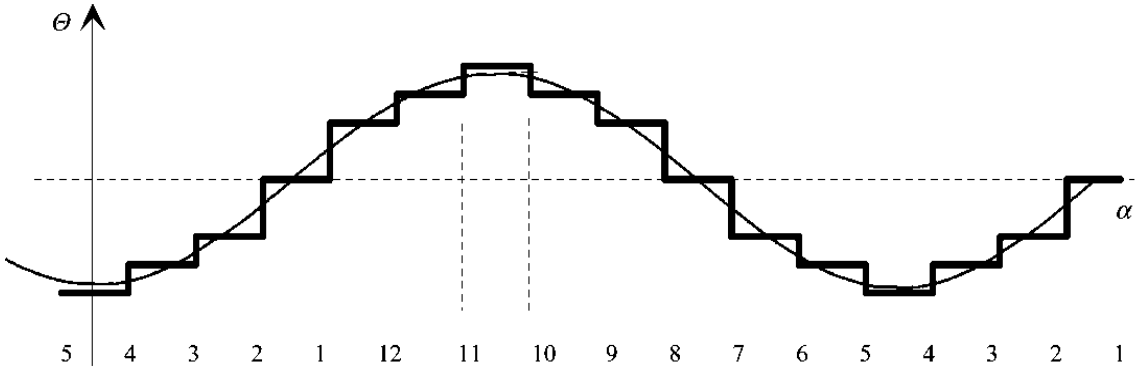

Fig. 12 Current linkage of the winding with the following parameters: $Q = 12$, $m = 3$, $p = 1$ and $q = 2$ and at the same moment of time as in Fig. 12. Modified from Design of Rotating Electrical Machines [2]

The form of the current linkage alters as the function depends on time, but in can be considered as a sine wave with presence of certain harmonics in future analysis.

Authors in [2] claim that the following equations can be used for calculating current linkage fundamental component and the ν^{th}-harmonic component respectively of m-phase rotating field winding:

$$\widehat{\Theta}_1 = \frac{m}{2}\frac{4}{\pi}\frac{Nk_{w1}}{2p}\sqrt{2}I, \tag{7}$$

$$\widehat{\Theta}_\nu = \frac{m}{2}\frac{4}{\pi}\frac{Nk_{w\nu}}{2p\nu}\sqrt{2}I\ . \tag{8}$$

Eq. 7 and Eq. 8 show that the amplitude of the ν^{th}-harmonic depends mainly on the stator current, number of phases, number of pole pairs and winding factor. The winding factor is the most complicated for determination. This part of Eq. 7 and Eq. 8 will be observed further.

1.6.3 Winding factor

Winding factor is a coefficient which is applied in taking into account the spatial distribution of the winding in slots on the stator surface. It also can be interpreted that the flux (or current linkage) does not cross all windings simultaneously. That is why the winding factors of harmonics are required. Better explanation of the physical meaning of winding factor can be obtained by employing voltage phasor diagrams. Electrical degrees are used when phasor diagrams are build [2]. Phasor diagram shows the voltages distribution in the winding conductors. Fig. 13 taken from [2] shows the voltage phasor diagram for machine with m = 3, p = 2, q = 1, and Q = 12.

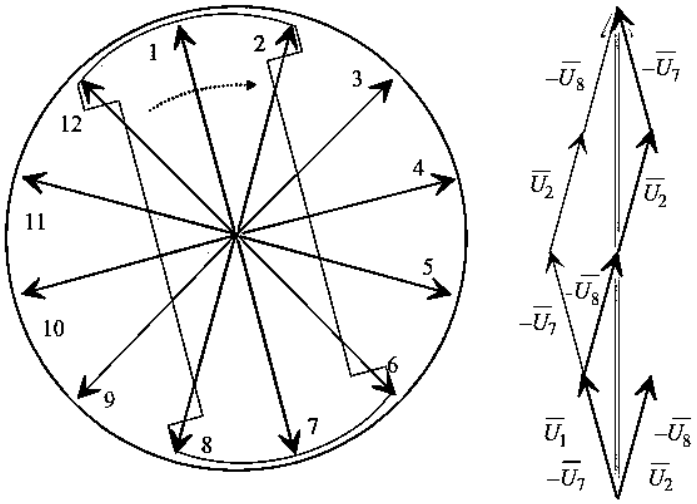

Fig. 13 Voltage phasor diagram for winding fundamental component with Q = 12, m = 3, p = 1, and q = 2. Modified from Design of Rotating Electrical Machines [2]

Drawing phasor diagram of fundamental component was made according to the explanations in [2].

Generally, the winding factor of the v^{th} -harmonic can be calculated by using the phasor diagram according to:

$$k_{\text{w}\nu} = \frac{geometric\ sum\ of\ phasors\ of\ \nu\text{th}\ harmonic}{sum\ of\ absolute\ values\ of\ phasors\ of\ the\ \nu\text{th}\ harmonic} \ . \tag{9}$$

For the future analysis good approximate result can be obtained by using Eq. 2.23, Eq. 2.25 and Eq. 4.21 from [2]. As a result the following equation gives approximate value

for winding factor of v harmonic (all parameters, used in this equation estimated during design process):

$$k_{\mathrm{w}}(v) = \frac{2\sin\left(v\frac{\pi}{2}W_{\tau\mathrm{p}}\right)\sin\left(\frac{v\pi}{2m}\right)}{\frac{Q}{mp}\sin(v\pi\frac{p}{Q})}\frac{\sin(v\frac{\pi D_{\mathrm{S}}\pi}{\tau_{\mathrm{p}}Q\ 2})}{v(\frac{\pi D_{\mathrm{S}}\pi}{\tau_{\mathrm{p}}Q\ 2})}. \quad (10)$$

1.6.4 Harmonics of current linkage

Current linkage of the slot winding can be presented by function $\theta = \mathrm{f}(\alpha)$ propagating in the machine's equivalent air gap. According to observations from [2], current linkage is not sinusoidal function and changes all the time due to low order harmonics. Authors in [2] give the following equation for determination the main harmonics created by an m-phase winding:

$$v = +1 \pm c2m, \quad (11)$$

where $c = 1,2,3\ldots$

Thus, a 3-phase integral slot winding creates harmonics presented in the Table 2.

Table 2 Main harmonics of the current linkage created by 3-phase winding.

c	0	1	2	3	4	5	6	7
ν	+1	+7	+13	+19	+25	+31	+37	+43
	-	–5	–11	–17	–23	–29	–35	–41

Data in Table 2 shows significant presence of low order harmonics. Harmonics with the negative sign propagate in the opposite direction from the fundamental. It can be also mentioned that there are no even harmonics and no harmonics multiple of 3 [2]. By taking Eq. 8 into account it can be concluded that the current linkage amplitude of the v^{th}-harmonic is inversely proportional to ordinal v of the harmonic. That is why at least the -5^{th} and 7^{th} harmonics should be considered in analysis of the current linkage, created by a 3-phase winding.

1.7 Short circuits in PMSMs

Permanent magnet synchronous machines have become more and more popular today due to their high power density, high efficiency and high torque to current ratio. However, a big problem for a PMSM is the possibility of the short circuit. PMSMs have rotor surface or buried magnets in their construction, and these magnets can be partially or fully irreversibly demagnetized during a short circuit by the armature reaction. This should mean a significant reduction of the machine performance and efficiency. The term "irreversible demagnetization" in this context means that properties of the PM become worse comparing to the initial state. Detailed description of the PM demagnetization provided above allows to conclude that the working point of the PM falls below the linear part of the original *BH*-curve. Now the behaviour of the PM is described by one of the recoil lines [3]. It is necessary to mention that, in principle, the PM can be re-magnetized again by applying very-high magnetic field strength, but in most cases it is impossible to do it without disassembling the rotor. Basically, the effect of short circuit on a permanent magnet can be described as follows: First, the operation point of the magnet can move below the linear zone due to increasing stator current caused increasing armature reaction. Second, the magnet can be partly or totally demagnetized from significant temperature rise and high demagnetizing stator current linkage. Detailed analysis of the first phenomenon will be considered further.

Mostly, papers about magnetic field analysis during short circuit are based on FEM analyses, which can give very accurate results, but are very time consuming. During the design of an electrical machine there is a need to estimate the approximate risk of the magnet demagnetization. But still no good analytical approach has been developed. In [11] analytical calculation of partial demagnetization has been derived based on synthesized magneto motive force and in detail consideration this method requires firstly data from FEM program analysis which makes this method not appropriate for fast calculation. According to the paper [11] an important conclusion could be made: average magnet operating point cannot describe the demagnetization risk of the whole magnet, and thus cannot be used for an accurate analytical approach.

1.7.1 Analytical approach in short circuit analysis

Symmetrical short circuit (SSC) currents in steady state are well known, but analysis of the currents' transient behaviour have not been performed yet with sufficient accuracy.

This behaviour strongly depends on the operating point of the motor at the moment of time when short circuit occurs. During the short circuit negative *d*-axis current can be so high that partial or total demagnetization of permanent magnets can take place. Approximate calculation of short circuits should be derived and operating points with the highest risk of possible demagnetization should be determined during design process [12]. In this section, first, analytical estimation of SSC currents has to be provided in case of neglecting the ohmic voltage drop. Next, general model for determination of the three-phase symmetrical short circuit currents will be presented. All these models are based on information from [12].

1.7.2 SSC model neglecting stator resistance

When theoretical analysis is provided, very often stator resistance is considered as part of supplying network resistance. In this paragraph the stator resistance is neglected for simplification of the model, but later it will be estimated, that this resistance plays a significant role in the behaviour of short circuit currents. Fig. 14 based on data from [12] shows a vector diagram of PMSM in case of short circuit. The following abbreviations are used in Fig. 14: ψ_x and ψ_y is the stator reference frame, ψ_{p0} is PM flux space vector in steady state, ψ_0 is the stator flux linkage space vector in steady state, $L_d i_{d0}$ and $L_q i_{q0}$ is the armature caused flux linkage space vectors in *d*- and *q*-axis respectively in normal operational mode, $\psi_p(t)$ is PM flux linkage space vector at random moment of time *t* after the short circuit occurred, $\Delta\psi(t)$ is a difference space vector between ψ_0 and $\psi_p(t)$, ψ_{pmax} is the PM flux linkage space vector at the time when $\psi_p(t)$ and ψ_0 directed exactly against each other, $L_d i_{dmax}$ is the maximum negative *d*-axis flux linkage space vector at the time when $\psi_p(t)$ and ψ_0 directed exactly against each other, α is the angle between the stator reference frame and PM flux space vector, β is angle between stator reference frame and ψ_0.

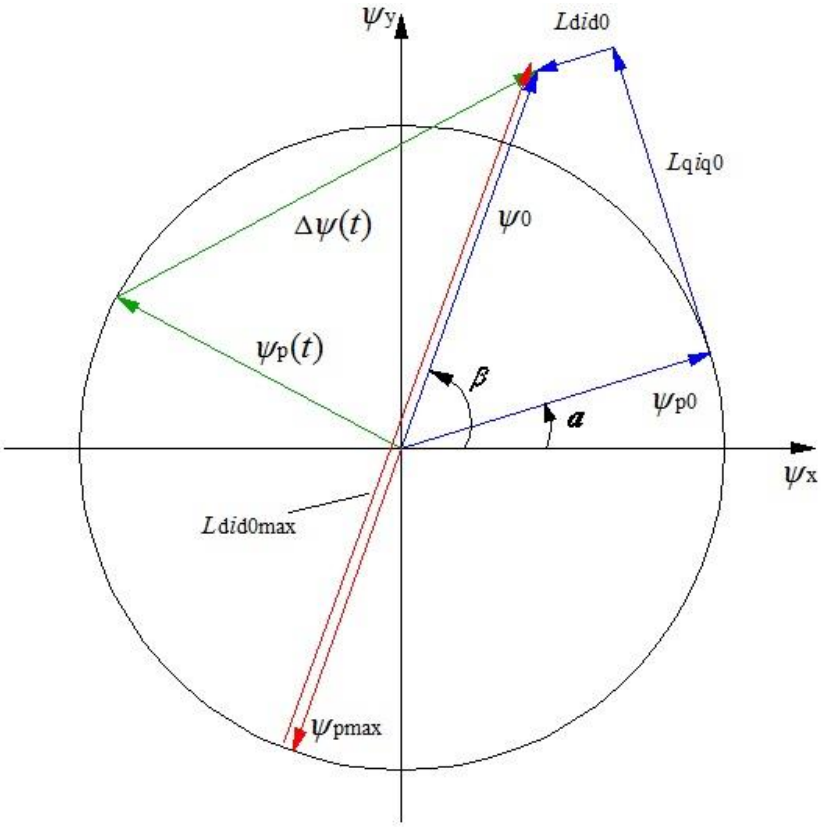

Fig. 14 Vector diagram of PMSM in case of short circuit. When three-phase SSC takes place the stator flux linkage space vector ψ_0 remains fixed in the stator reference frame. The PM flux space vector $\psi_p(t)$ continue to move from its initial position ψ_{p0} with rotor electrical speed ω_R for sufficient time. The worst situation for the magnet occurs when the stator flux linkage space vector $\psi_p(t)$ is directed exactly opposite to the PM flux space vector ψ_0.

In stator fixed XY reference frame, the following equations describe the voltage equations of a PMSM:

$$u_x = Ri_x + d\psi_x/dt, \tag{12}$$

$$u_y = Ri_y + d\psi_y/dt. \tag{13}$$

In Eq. 12 and Eq. 13 u_x, u_y, i_x, i_y, ψ_x and ψ_y are X- and Y- components of the stator voltage space vector, stator current space vector and stator flux space vector in the stator fixed reference frame. If saturation effects are not taken into account, the following equations can express the stator flux linkage vector $\boldsymbol{\psi}$ components in the stator fixed XY reference frame:

$$\psi_x = \cos(\alpha)(\psi_{PM} + L_d i_d) + \sin(\alpha)(L_q i_q), \tag{14}$$

$$\psi_y = -\sin(\alpha)(\psi_{PM} + L_d i_d) + \cos(\alpha)(L_q i_q). \tag{15}$$

The voltage equations in the rotor fixed reference frame are:

$$u_d = L_d i_d + R i_d - \omega_R L_q i_q, \tag{16}$$

$$u_q = L_q i_q + R i_q + \omega_R L_d i_d + \omega_R \psi_{pm}, \tag{17}$$

where ω_R is the rotor rotating electrical angular frequency and ψ_{pm} is the absolute value of the flux linkage of the permanent magnets created in the stator winding. When 3-phase short circuit occurs, terminal voltages are equal to zero:

$$u_x = u_y = 0. \tag{18}$$

Eq. (12), Eq. (13) and Eq. (18) show that in case of short circuit the change of the stator flux in the stator coordinate system is determined by the ohmic voltage drop. As it was previously said in this paragraph, the stator ohmic losses and core losses have been neglected. This assumption means that the stator flux linkage remains fixed and unchanged in the stator reference frame from the instant when the short circuit occurred. It is assumed that the short circuit occurs at time $t = 0$. Further, all quantities related to this time instant are subscripted with "0". The following equations show the values for the permanent magnet flux linkage and the stator flux linkage at time instant $t = 0$:

$$\boldsymbol{\psi}\,(t = 0) = \boldsymbol{\psi}_0 = |\boldsymbol{\psi}_0| \angle \beta, \tag{19}$$

$$\boldsymbol{\psi}_{PM}\,(t = 0) = \boldsymbol{\psi}_{p0} = |\,\boldsymbol{\psi}_{p0}| \angle\, \alpha. \tag{20}$$

Next, assumption that the rotor keeps its angular speed during relevant period in the first moment should be made. This assumption results in that the permanent magnet flux linkage vector keeps on turning with the rotor electrical rotating frequency ω_R. The behaviour of the permanent magnet flux linkage and stator flux linkage vectors after the short circuit occurs, and according to the above assumptions are:

$$\boldsymbol{\psi}(t \geq 0) = \boldsymbol{\psi}_0, \tag{21}$$

$$\boldsymbol{\psi}_{PM}(t \geq 0) = \boldsymbol{\psi}_{\,p} \angle\, (\alpha + \omega_R t). \tag{22}$$

This observation leads to an idea, that the evolution of the current $i(t)$ can be obtained from the difference vector between the "stationary" stator flux linkage space vector and the rotating permanent magnet flux linkage space vector:

$$\Delta\boldsymbol{\psi}\,(t) = \boldsymbol{\psi}_0 - \boldsymbol{\psi}_{\mathrm{PM}}(t). \tag{23}$$

From Fig. 14 and Eq. (21 - 23) time $t_{\max}$ is corresponding to the worst case for permanent magnet and can be calculated as:

$$t_{\max} = \frac{\beta + \pi - \propto}{\omega_{\mathrm{R}}}. \tag{24}$$

Orientation of $\Delta\psi$ ($t_{\max}$) has the negative *d*-direction, so it can result in serious risk of the permanent magnet demagnetization. Vectors i_{d} and i_{q} could be calculated by:

$$\boldsymbol{i}_{\mathrm{d}} = \frac{\Delta\boldsymbol{\psi}_{\mathrm{d}}}{L_{\mathrm{d}}}, \tag{25}$$

$$\boldsymbol{i}_{\mathrm{q}} = \frac{\Delta\boldsymbol{\psi}_{\mathrm{q}}}{L_{\mathrm{q}}}. \tag{26}$$

Summarizing the above observations and assumptions the following equations could be used for determining the *d*-axis and *q*-axis currents in the beginning of a three-phase symmetrical short circuit:

$$i_{\mathrm{d}}(t) = -\frac{\boldsymbol{\psi}_{\mathrm{p}}}{L_{\mathrm{d}}} + \frac{|\boldsymbol{\psi}_0|}{L_{\mathrm{d}}}\cos(\omega_{\mathrm{R}}t + \alpha - \beta), \tag{27}$$

$$i_{\mathrm{q}}(t) = -\frac{|\boldsymbol{\psi}_0|}{L_{\mathrm{d}}}\sin(\omega_{\mathrm{R}}t + \alpha - \beta). \tag{28}$$

1.7.3 SSC model which takes into account the stator resistance

In practice, the stator resistance cannot be neglected due to its significant influence on the stator flux linkage behaviour. That is why the model proposed above now will be observed taking into account stator ohmic voltage drop. In this case Eq. 12 and Eq. 13 can be rewritten in the following way:

$$\psi_{\mathrm{x}} = -Ri_{\mathrm{x}}, \tag{29}$$

$$\psi_{\mathrm{y}} = -Ri_{\mathrm{y}}. \tag{30}$$

Eq. (29) and Eq. (30) show that in case of existing stator ohmic voltage drop (which takes place in practice) the stator flux linkage vector will not stay fixed in the stator oriented coordinates any more. Voltage drop makes the stator flux linkage rotate in the opposite direction from the stator current vector. It should be mentioned also that the stator current

vector causes decreasing of the stator flux vector to its steady state value which is characterized by the transient process.

The following assumptions are made: motor retains the constant speed during relevant time after the short circuit, saturation of magnetic circuit is neglected. Then Eqs. 16–18 can give determination of the *d*- and *q*- axis currents as following:

$$i_{\mathrm{d}}(t) = e^{-\frac{t}{\tau}} K_{\mathrm{d}} \cos(\varphi_{\mathrm{d}}(t)) + i_{\mathrm{d.ss}}, \tag{31}$$

$$i_{\mathrm{q}}(t) = e^{-\frac{t}{\tau}} K_{\mathrm{q}} \cos\big(\varphi_{\mathrm{q}}(t)\big) + i_{\mathrm{q.ss}}. \tag{32}$$

Eq. (31) and Eq. (32) were found in [12]. These equations were obtained from computer algebra program and were presented in [12] without derivation. Here, $i_{\mathrm{d.ss}}$ and $i_{\mathrm{q.ss}}$ are the steady state short circuit currents while $\exp(-t/\tau)K_{\mathrm{i}}$ describes the decaying magnitudes of the transient current components.

The steady state SSC currents can be calculated as following [12]:

$$i_{\mathrm{d.ss}} = -\frac{L_{\mathrm{q}}\omega_{\mathrm{R}}^2\psi_{\mathrm{p}}}{R^2 + \omega_{\mathrm{R}}^2 L_{\mathrm{d}} L_{\mathrm{q}}}, \tag{33}$$

$$i_{\mathrm{q.ss}} = -\frac{R\omega_{\mathrm{R}}^2\psi_{\mathrm{p}}}{R^2 + \omega_{\mathrm{R}}^2 L_{\mathrm{d}} L_{\mathrm{q}}}. \tag{34}$$

The decay time constant τ is given as following:

$$\tau = \frac{2L_{\mathrm{d}}L_{\mathrm{q}}}{R(L_{\mathrm{d}} + L_{\mathrm{q}})}. \tag{35}$$

Other components of Eq. 31 and Eq. 32 can be derived based on the assumption that for a sufficiently high speed

$$\omega_{\mathrm{R}}^2 >> R^2 / L_{\mathrm{d}}L_{\mathrm{q}}, \tag{36}$$

the stator flux linkage vector angle β remains unchanged, while the vector magnitude decreases with the time constant τ:

$$\beta(0) = \beta(t),\ t > 0. \tag{37}$$

The approximate values for other components of Eq. (31) and Eq. (32) can be obtained from Eq. (27) and Eq. (28) (in these equations stator ohmic voltage drop is neglected):

$$K_{\mathrm{d}} = \frac{|\boldsymbol{\psi}_0|}{L_{\mathrm{d}}}, \tag{38}$$

$$K_{\mathrm{q}} = \frac{|\boldsymbol{\psi}_0|}{L_{\mathrm{q}}}, \tag{39}$$

$$\varphi_{\mathrm{d}}(t) = \omega_{\mathrm{R}} t + \alpha - \beta, \tag{40}$$

$$\varphi_{\mathrm{q}}(t) = \omega_{\mathrm{R}} t + \alpha - \beta + \frac{\pi}{2}. \tag{41}$$

If assumptions in Eq. (36) and Eq. (37) are true, than Eq. (31), (32), (38 – 41) give analytical approximation of the transient current. Accuracy of the proposed equation need to be validated by FEM-based program in the next section of this thesis.

1.7.4 The worst case short circuit

According to Fig. 14 the worst situation for a permanent magnet happens at the time when the stator flux linkage vector and the permanent magnet flux linkage vector have exactly opposite directions. Eq. 31 and Eq. 32 show that the highest amplitude of the SSC current happens at the first time when $\cos(\varphi_{\mathrm{d}}(t_{\max})) = -1$ after short a circuit took place. Summarizing the above observations, the maximum magnitude of the transient short circuit currents can be estimated:

$$i_{\max} = i_{\mathrm{d\,max}} = -\frac{\boldsymbol{\psi}_{\mathrm{p}}}{L_{\mathrm{d}}} - \frac{|\boldsymbol{\psi}_0|}{L_{\mathrm{d}}} e^{-\frac{t_{\max}}{\tau}}. \tag{42}$$

The most negative stator flux value in *d*-direction is calculated as follows:

$$\psi_{\mathrm{d\,min}} = -|\boldsymbol{\psi}_0| e^{-\frac{t_{\max}}{\tau}}, \tag{43}$$

where ψ_{PM}, L_{d} and τ are obviously determined during the design process of the electrical machine, and thus these parameters do not depend on the operating point. However, $|\psi_0|$ and $t_{\max}$ depend on the operating point and speed of the motor. The higher the stator flux linkage magnitude is the worse short circuit current behaviour will results [12]. The difference between β and α angles shows the orientation of the stator flux linkage vector ψ in the rotor fixed coordinates. Decreasing angle β and rising of ω_{R} decrease $t_{\max}$. [12]

Analysis in [12] shows that the negative effect of the short circuit increases with decreasing angle β, increasing speed ω_R and increasing stator flux linkage vector.

1.7.5 Influence of the iron saturation on magnetic circuit

Authors in [12] state that despite of extremely high values of the SCCs the total stator flux linkage is not increasing and, moreover, it is decreasing due to the stator currents. This phenomenon is explained by the fact that the SSC currents flowing in the stator try to recoup the difference between the PM flux linkage and the stator flux linkage. As it was previously mentioned, when SSC takes place the stator flux linkage space vector is assumed to be motionless while the PM flux linkage space vector is rotating with rotor electrical speed. This allows to conclude that no unusual effects of the saturation are expected in the stator. Authors in [12] state that saturation can take place in the rotor of the PMSM because of the very high magnetic flux density in the moment of the time when stator flux linkage is directed in the *d*- direction.

2 RESEARCH THEORETICAL DEVELOPMENT

Predicting of the magnetic flux density distribution in the PMSMs has always been a very demanding task. Basically, many things can be analysed quite accurately if the magnetic flux density of the machine is known. Analysis of this problem shows that it is very difficult to calculate the flux density of the machine with simple models because of a large number of parameters which are involved in this phenomenon. These parameters can be geometric, physical, electrical and magnetic. The problem is further complicated by the fact that the machine can work in different operational modes. In each mode the magnetic flux density distribution will be different. Because of the extreme difficulty of the problem special FEM software programs have been developed. The working principle of such a software is based on dividing the whole magnetic circuit in many parts – finite elements. The magnetic properties of each part can be considered linear or can be described with a polynomial equation. Then the software solves a very big amount of equations based on the Maxwell´s equations and Dirichlet and Neumann boundary conditions. This is assumed as the best and the most accurate method for the electrical machine analysis. The disadvantages of this method are long calculation time, relatively long process of putting parameters of the machine in FEM program. It can be also mentioned that due to fast developing of computers the calculation time will be not a problem in the future, but still there is demand for simple and quite accurate models to analyse the magnetic field without FEM software.

Next, the parameters which have to be determined should be described. Analysis of the theory shows that problems related to the PM can be predicted, analysed and avoided only by determining the magnetic flux density in every point of the magnet. This means that prediction of PM flux density distribution is very important task.

Analysis of the literature [2] and [13] shows that many parameters have to be used as input parameters in the proposed model. These parameters should describe the magnetic properties of the PM and the iron which is used as part of the magnetic circuit. Constructional iron parts of the electrical machine, of course, have influence on the final properties but this influence is neglected in the model proposed. Magnet´s shape, magnetic properties and location in the rotor cannot be neglected either. Data from [14] and [15] shows noticeable difference in magnetic properties between surface mounted

magnets with different direction of the magnetization. This difference in the magnetic properties is most noticeable exactly at the edges of the PM. As it was previously said hysteresis losses during the normal operational mode may occur only in the parts of the magnet whose magnetic flux density intermittently goes higher than the remanent flux density. Analysis of theory presented in [1] and observations from FEM based programs show that one of the PM edge is prone to hysteresis losses more than other parts of the PM. That is why the magnetization direction of the magnet cannot be neglected.

The working conditions of the machine play also important role. The theory presented in [2] shows that saturation of parts of the magnetic circuit should be avoided in design process of the electrical machine. If the saturation of iron is avoided then the assumption that magnetic circuit is linear could be made. Very often in fast approaches it is assumed that the relative permeability of the iron is infinite. This assumption allows to neglect the magnetic voltage drop in iron part of the magnetic circuit. Data from [2] shows that in principle, the magnetic voltage drop cannot be neglected and should be taken into account. According to the observations from FEM software and data from [2] the magnetic voltage drop in the iron part of the magnetic circuit can be taken into account as 1-5 % of overall magnetic voltage of the whole magnetic circuit. This is an important observation which easily allows to evaluate quite complicated phenomena.

Armature winding is the most complicated system which has to be taken into account during the magnetic flux density evaluation. The no-load air gap flux density which, in principle, should not be very different from the PM flux density was accurately described in [14] – [16]. As the result the cogging torque of the machine calculated with analytical approach presented in [15] matches pretty well with FEM program results. But still very few articles have been published about analytical evaluation of the armature reaction even in normal operational mode of the electrical machine. This problem of the evaluation of armature reaction field is very complicated because of too many parameters that have to be taken into account during analytical approach. Even in three phase supply system the windings of the electrical machines have different constructions, resulting in different current linkage and harmonic contents. The regime of PMSM operation has significant effect on the resulting armature winding current linkage. Operational regime parameters are known during the normal operational mode. But in the case of a short circuit (even if it is a three-phase short circuit) the task of the predicting the resulting magnetic flux

density in the magnet becomes extremely difficult. Analysis of the literature shows that no good analytical approach for the short circuit theory has been provided yet. The SSC current can be modelled with sufficient accuracy according to the theory presented in [12]. It should be mentioned that accuracy of the methods proposed in [12] is increasing with increasing of the speed of the SM. It is very good because the PMSMs are more often designed for higher speeds nowadays.

The theory presented in [2] and [13] provides the necessary basis for the magnetic flux density estimation in the air gap and PM of the PMSMs. The proposed model is based on the space vector theory presented in [13] and common theory of the magnetic circuits presented, for example, by Pyrhönen *et al.* in [2].

First, assumptions used in the proposed model which are based on the space vector theory should be considered. As was previously stated, the literature [14], [16] and [15] provide good and accurate analytical approach for no-load magnetic flux density estimation in rotor-surface magnet PMSMs with different direction of the magnetization. The most difficult thing which has not been described analytically yet is the armature reaction. Theory presented by Pyrhönen *et al.* in [2] states that armature reaction caused by armature current linkage is changing all the time because of the harmonics which are produced by the winding. Moreover, in the normal operational mode the current linkage of the armature winding has to rotate with the rotor speed. The space vector theory presented, for example, in [13] allows to represent any current, voltage or flux linkage of the rotating field machine as vector in the respective reference frame but taking only the fundamental into account. If the rotor of the SM is in the steady state then the armature reaction of the stator winding can be represented as two vector components in the rotor reference frame (as well as in any other reference frame). It also should be mentioned that space vector theory can be used during the transients and this feature will be used further. The main source of the armature reaction are the currents which are flowing in the stator winding. This phenomenon cannot be avoided due to the working principle of the rotating field machines because armature winding is essential part of the machine and its main task is the energy transition to or from the external system. It is assumed in the model that the stator is motionless and rotor is rotating with its electrical speed. If consider the rotor in the rotor reference frame then at least current linkage fundamental component of the stator winding can be represented as two vectors. The first current vector is equivalent to

magneto motive force created by the stator winding and directed exactly along *q*- axis of the magnet. The second current vector is directed along direction of the *d*- axis of the magnet. The amplitude of the fundamental, as well as any other harmonic, and total harmonic content can be determined according to the theory presented in the first chapter. The harmonic content created by the stator armature winding will not move with the speed of fundamental. However, if it is assumed that during the time of the model observation all the harmonic component phase shifts are equal to zero, then it is possible to obtain resulting current linkage of the stator winding at the certain moment of time.

The current linkage created by the armature winding is presented in model as the sum sine wave of the fundamental component and harmonic content. The magnitudes of these components are determined with Eqs. (7-8) and the harmonics are determined according to the data presented in Table 2. It is very important to mention that, in principle, the current linkage of the armature winding is not a sinewave. Theory presented by Pyrhönen *et al.* in [2] states that the current linkage looks like the stepped curve because of the effect of the stator slotting. This fact can seriously limit the accuracy of the proposed model in applications with extremely high armature reaction. Literature analysis and the observations of the FEM based programs show that in most cases the PMs in PMSMs are the largest sources of the magnetic flux density. The armature reaction of the armature winding cannot be neglected but it usually can create current linkages smaller than those created by the PMs. This fact allows to neglect the effect of the stator slotting of the armature winding when analysis of current linkage is provided and still to obtain accurate results. It needs to be borne in mind, that the effect of the stator slotting cannot be neglected in the magnetic resistance analysis of the magnetic circuit.

The proposed model represents the PMSMs with rotor-surface mounted magnets as magnetic circuit consisting of two sources of the flux and four linear magnetic resistances. The sources of the fluxes are the *dq*- current linkages of the stator armature winding and the PMs. The magnetic resistances in the model are assumed to be connected in parallel. The most complicated resistance for the modelling is the stator slot and slot opening resistance.

The reliability of the magnet´s operation has to be checked not only in normal operational mode. The most dangerous mode from the PM´s point of view is short circuit but still no

good theory have been presented for different short circuit types calculations. Even SSC according to the theory presented in Chapter 1 allows to calculate short circuit currents with ca. 15% inaccuracy. Moreover, the magnetic circuit cannot be considered as linear in case of short circuit due to extremely high currents in the armature winding. Thus, the accurate PM magnetic flux density determination during the various short circuits is very challenging task.

3 APPLICATION OF THE THEORY

The implementation of the research is based on solving the simple equations of the magnetic circuit and vector diagrams of the PMSM. All parameters that are used in the model were previously defined during the design process. First, the vector diagram of the PMSM in *dq*- reference frame should be observed. This vector diagram was build according to the space vector theory and is presented in Fig. 16, [13].

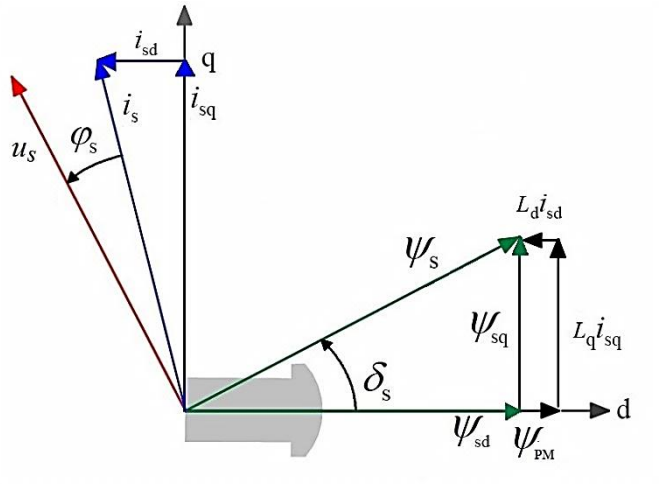

Fig. 16 Vector diagram of a PMSM. Modified from [13]

Part of this figure representing the stator flux linkage is quite similar to the stator flux linkage in Fig. 15. Fig. 16 shows that the stator voltage, all fluxes and currents of the PMSM can be represented by respective *d*- and *q*- components. For example, the stator flux linkage ψ_s can be represented through its ψ_{sq} and ψ_{sd} components. Similarly, the stator current vector can be represented with its i_{sq} and i_{sd} components. This space vector diagram was built in the rotor reference frame and this means that it is rotating with the rotor angular speed. But at the same time this means that all the space vectors are stationary to each other with the same magnitudes and angles [13]. This is true, of course, if the operational mode is steady. According to the theory from Chapter 4, the current linkage of the stator winding can be expressed as a sine wave with a certain content of harmonics. This observation allows making an assumption that the stator winding current linkage can be replaced by two separate windings. Summarizing observations about the stator winding current linkage from Chapter 4 and space vector diagram from Fig. 16 the stator winding can be represented by two imaginary windings, one winding creates current linkage only in *d*- axis (corresponds to i_{sd} space vector) and the another winding creates current linkage only in *q*- axis (corresponds to i_{sq} space vector).

It is good to mention here that as the result of the design process the following values are usually determined for the normal operational mode: load angle δ_s, angle determining the power factor of the PMSM, φ_s, *d*- and *q*- axis inductances, stator currents in d*q*- reference frame i_{sq} and i_{sd}. These values allow to calculate all the other components of the PMSM space vector diagram with the use of simple geometric calculations easily. This makes the task of calculating the three-phase short circuit easier. Here it should be mentioned that all the spatial quantities are assumed sinusoidal in the space vector theory [13], so this method allows to calculate only the fundamental flux related components. In practice, there is significant presence of the low order space harmonics that distorts the air gap flux density.

Based on the information presented in Fig. 16 the PM flux linkage space vector magnitude can be calculated as:

$$\boldsymbol{\psi}_{\mathrm{PM}} = -I_{\mathrm{d}}L_{\mathrm{d}} + \frac{I_{\mathrm{q}}L_{\mathrm{q}}}{\tan(\delta_{\mathrm{s}})}. \tag{44}$$

The stator flux linkage space vector magnitude can be calculated as:

$$\boldsymbol{\psi}_0 = \sqrt{(\boldsymbol{\psi}_{\mathrm{PM}} + I_{\mathrm{d}}L_{\mathrm{d}})^2 + (I_{\mathrm{q}}L_{\mathrm{q}})^2}. \tag{45}$$

Eq. 44 and Eq. 45 can be used together with the short circuit theory presented in Chapter 5.

Next, the general model for magnetic flux density calculation is be presented. The idea of the model is that for a synchronous machine in a steady state all the values (stator current space vectors, stator flux linkage space vector PM flux space vector, and stator voltage space vector) are motionless with respect to each other. This allows to depict the pole of the PMSM as it shown in Fig. 17:

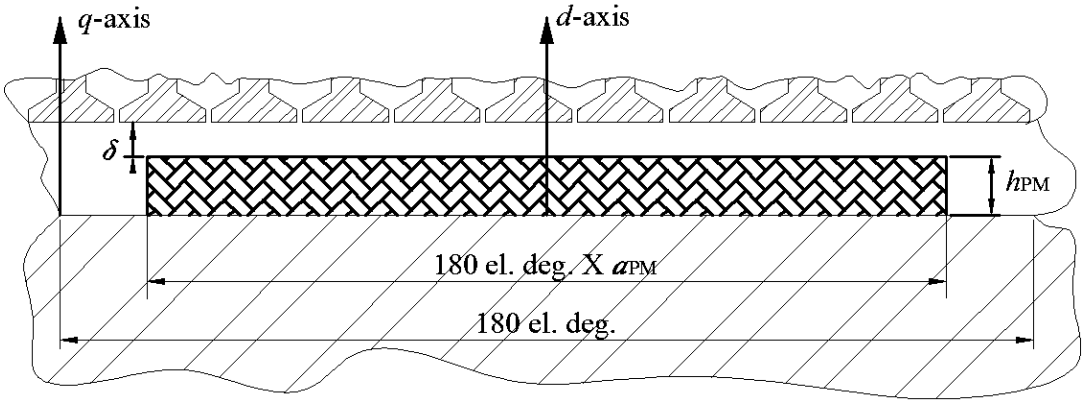

Fig. 17 The proposed model for the magnetic flux density analysis in the PMSM

Fig. 17 depicts one pole of the surface PMSM. From the literature analysis it can be concluded that the main factor affecting the air gap flux density distortion is the armature reaction [2]. With the theory from Chapter 4 and space vector diagram in Fig. 16 the stator winding current linkage can be divided into two separate parts. The first part of the stator current linkage creates almost sinusoidal current linkage (of course, with the presence of some low order harmonics) in the *d*-axis direction. In normal operation mode *d*-axis current is often slightly demagnetizing [2], so the *d*-axis current linkage will try to demagnetize the PM. The second part of the stator current linkage creates a positive almost sinusoidal current linkage in the *q*-axis direction. This part of current linkage contains current component responsible for the torque production of the non-salient-pole PMSM [13]. The influence of this *q*-axis current linkage component should be observed with the proposed model.

Calculation of the magnetic flux (and the magnetic flux density respectively) requires the knowledge of the PMSM magnetic resistances. According to the proposed solution the model is divided into four separate "layers" as shown in Fig. 18:

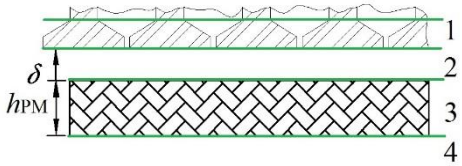

Fig. 18 Division of the surface PMSM into four layers with different magnetic resistances. 1. Stator tooth region, 2. Physical air gap, 3. Permanent magnet, 4. Rest of the magnetic circuit

The first layer in Fig. 18 represents the slots and the slot openings of the PMSM. Usually, the magnetic wedges are used in the slot openings. The main function of the magnetic

wedges is to reduce the effective stator slot opening and distortion of the air-gap flux density in the PMSMs and in other rotating field machines [17]. Even with wedges manufactured from semi-magnetic material the slot openings have a significant influence on the magnetic flux density behaviour, causing decrease of the flux density [2]. The second layer depicts the air gap of the PMSM. The third layer describes the PM. The fourth layer shows all remaining iron parts of the magnetic circuit: stator and rotor yokes and remaining parts of the teeth.

Now, the basics of the theory describing the proposed model have been presented. In the following paragraphs every part of the model is described in details.

3.1 Input parameters

In this paragraph the input parameters for the proposed solution are presented. First, input parameters for the normal operation mode are described. However, in case of short circuit some extra parameters of the machine are required. These parameters are described in the second part of this subsection.

3.1.1 Input parameters for normal operation mode

All parameters listed here are usually determined during the design process. The units are in square brackets.

P – shaft power of the PMSM, [W]

U – line-to-line RMS voltage, [V]

m – number of phases

$\cos\varphi$ – power factor of the PMSM

η – efficiency of the PMSM

The parameters, described above are required for the determination of the RMS value of the stator phase current. User can provide the stator current RMS value instead of the parameters listed above.

Next, the input parameters required for the correct stator winding current linkage determination are presented:

$W_{\tau p}$ – winding pitch

δ_s – load angle of the PMSM, [deg]

m – number of phases

D_s – inner stator diameter, [m]

τ_p – stator pole pitch, [m]

Q – number of stator slots

q – number of slots per pole and phase

p – number of pole pairs

N – number of coil turns in series per stator phase winding

The following parameters are required for the correct determination of the current linkage created by the PM:

H_c – coercive force of the PM material used in the machine, [A/m]

B_r – remanent flux density of the PM material used in the machine, [T]

D_r – the rotor diameter (including rotor surface magnets), [m]

α_{pm} – the physical relative magnet width

h_{pm} – the height of the PM, [m]

Moreover, the shape of the PM must be known because it has a significant influence on the magnetic flux density in the air gap.

Next, there is a list of parameters which are needed for accurate determination of magnetic resistances in the magnetic circuit of the machine:

δ – physical air gap length, [m]

The following slot dimensions should be determined in meters as it is shown in Fig. 19, taken from [2]:

b_1 – width of the slot opening, [m]

h_1 – height of stator tooth with constant width, [m]

h_2 – height of stator tooth, [8] as it is shown in Fig. 19

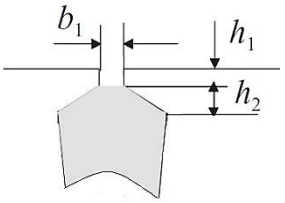

Fig. 19 Slot dimensions required for a proposed model. Modified from Design of Rotating Electrical Machines

3.1.2 Additional input parameters for the three-phase short circuit calculation

For the three-phase short circuit calculation the following parameters are required in addition to the parameters, described above:

R – DC resistance of a phase winding at rated temperature, [Ω]

L_d – *d*-axis inductance of the PMSM, [H]

L_q – *q*-axis inductance of the PMSM, [H]

These additional parameters are always determined with certain inaccuracy. Moreover, analysis of the literature [2] and [13] shows dependence of the resistance on the temperature, and the temperature can change very significantly during a short circuit. Inductances of the machine cannot be considered as constants either because they are saturated all the time [13]. This allows to conclude that a method based on resistances and inductances is not accurate but still can give an acceptable approximate solution.

3.2 Modelling of the current linkages

The modelling of the current linkages is performed according to the common theory of magnetic circuits presented, for example, in [2], [16] - [18].

3.2.1 Permanent magnet current linkage in the air gap

Analysis of the literature [2], [18], [14] shows that the current linkage of the permanent magnets strongly depends on its geometrical form, location of the PM in rotor and PM magnetization direction. Pyrhönen *et al.* in [19] presented data about flux density at the

ends of the PM with different length of the stator. This data allows to make a conclusion that if rotor and stator stacks are of the same length the current linkage of the rectangular PM in the air gap cannot be considered as rectangular because of the flux leakage on the edges of the magnet. Observations presented in [2], [18], [19] show that when modelling the current linkage of the PM the form of the PM, its location in the rotor, magnetization direction and the decreasing of current linkage at the edges due to flux leakage should be taken into account. First, the mathematical data adopted from [15] that allows to represent the air gap flux density of the surface magnet with the radial magnetization direction should be presented. In case of the slotless stator it can be expressed as:

$$B_{\mathrm{PM}}(x) = \sum_{\mathrm{n}=1,3,5\ldots}\left[\frac{4B_{\mathrm{r}}}{\mu_{\mathrm{r}}}\frac{\sin\left(\frac{n\pi\alpha_{\mathrm{PM}}}{2}\right)}{\pi}\frac{1}{(np)^2-1}\right]\left[\frac{(np-1)+2\left[\frac{(D_{\mathrm{r}}-2h_{\mathrm{PM}})}{D_{\mathrm{r}}}\right]^{np+1}-(np+1)\left[\frac{D_{\mathrm{r}}-2h_{\mathrm{PM}}}{D_{\mathrm{r}}}\right]^{2pn}}{\frac{\mu_{\mathrm{r}}+1}{\mu_{\mathrm{r}}}\left[1-\left[\frac{(D_{\mathrm{r}}-2h_{\mathrm{PM}})}{D_{\mathrm{r}}}\right]^{2np}\right]-\frac{\mu_{\mathrm{r}}-1}{\mu_{\mathrm{r}}}\left[1-\left[\frac{(D_{\mathrm{r}})}{D_{\mathrm{r}}+2\delta}\right]^{2np}\right]-\frac{(D_{\mathrm{r}}-2h_{PM})^{2np}}{D_{\mathrm{r}}}}\right], \left[\left(\frac{(D_{\mathrm{r}}+\delta)}{D_{\mathrm{r}}+2\delta}\right)^{np-1}\frac{D_{\mathrm{r}}}{D_{\mathrm{r}}+\delta}^{np+1}+\frac{D_{\mathrm{r}}}{D_{\mathrm{r}}+\delta}^{np+1}\right]\cos(npx) \quad (46)$$

where *x* is the location of the PM on the rotor surface in electrical degrees. Eq. (46) gives a very good approach for the rotor-surface-mounted PM air gap flux density but this equation should be modified to be able to simulate the rotor-surface-mounted PM current linkage. The following equation was obtained from Eq. (46) for the rotor-surface-mounted PM current linkage:

$$\Theta_{\mathrm{PM}}(x) = \sum_{\mathrm{n}=1,3,5\ldots}\left[H_{\mathrm{c}}h_{\mathrm{PM}}\sqrt{2}\sin\left(\frac{n\pi\alpha_{\mathrm{PM}}}{2}\right)\frac{1}{(np_1)^2-1}\right]\left[\frac{(np_1-1)+2[0.95]^{np_1+1}-(np_1+1)[0.95]^{2p_1n}}{2[1-[0.95]^{2np}]}\right]. [(0.95)^{2np_1}+0.95^{np_1+1}]\cos(np_1x) \quad (47)$$

All the coefficients in Eq. (47) were determined analytically. Detailed explanation of Eq. (47) is required here. Eq. (47) was derived from Eq. (46). Observation of the Eq. (46) shows that, generally, no-load flux density distribution in the air gap is a complicated function which depends on many parameters. It should also be mentioned that comparison of the resulting no-load flux density calculated with Eq. (46) not correspond to the results obtained from FEM program, so Eq. (46) cannot be used for calculation of no-load flux

density in the proposed model. The main advantage of the function presented in Eq. (46) is a good resulting shape of no-load magnetic flux density. This feature of the Eq. (46) is used in Eq. (47). The main objective of Eq. (47) is to create a function for description of the no-load air-gap flux density, but it should be done in proposed model. The only parameters which are used in the current linkage determination should be used in this equation. That means that only the coercive force, remanent flux density, height and relative width can be used as the input parameters. It also should be mentioned that such phenomenon as flux leakage from the edges of the magnet cannot be ignored when PM is located in the air gap a PM machine. Observations above allow to make a conclusion that there is a need to create function that have to depend only on PM parameters and take into account flux leakage effects on the edges of the PM. Eq. (47) satisfies the above requirements and has inaccuracy less than 1.7 % if relative PM width $\alpha_{PM} \geq 0.5$. More accurate verification should be provided with FEM program. Eq. (47) can be used for the analysis of every rotor-surface PM machine according to the proposed model. The parameter $p_1 = 1.001$ is used for preventing the dividing by zero is case when $np_1=1$. The input parameters in Eq. (47) are coercive force of the PM H_c, the physical height of the PM h_{PM} and the relative width of the magnet α_{PM}.

Fig. 20 shows the resulting current linkage over one pole created by the PMs with the same height but with different relative magnet width α_{pm} calculated according to the proposed solution.

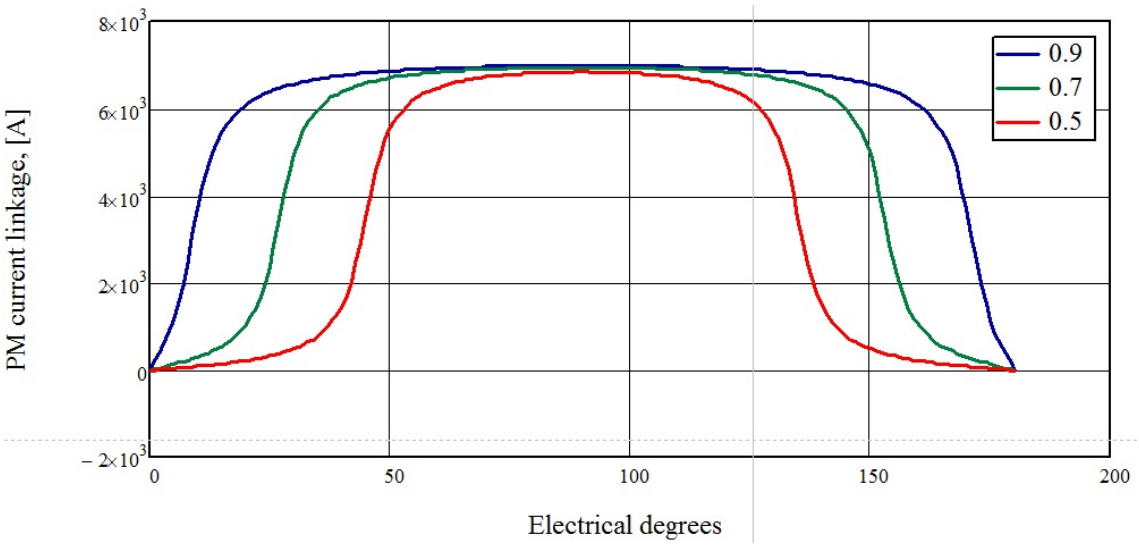

Fig. 20 Current linkage created by one PM for the PM with equal shape, height, location but with different relative PM width α_{pm} = 0.9, 0.7, and 0.5 respectively

Fig. 21 shows a comparison of the real rectangular current linkage and the virtual effective case calculated according to the proposed solution at the edges of the PMs with different relative widths α_{pm}. The results in Fig. 21 correspond well with data from [2] and [19].

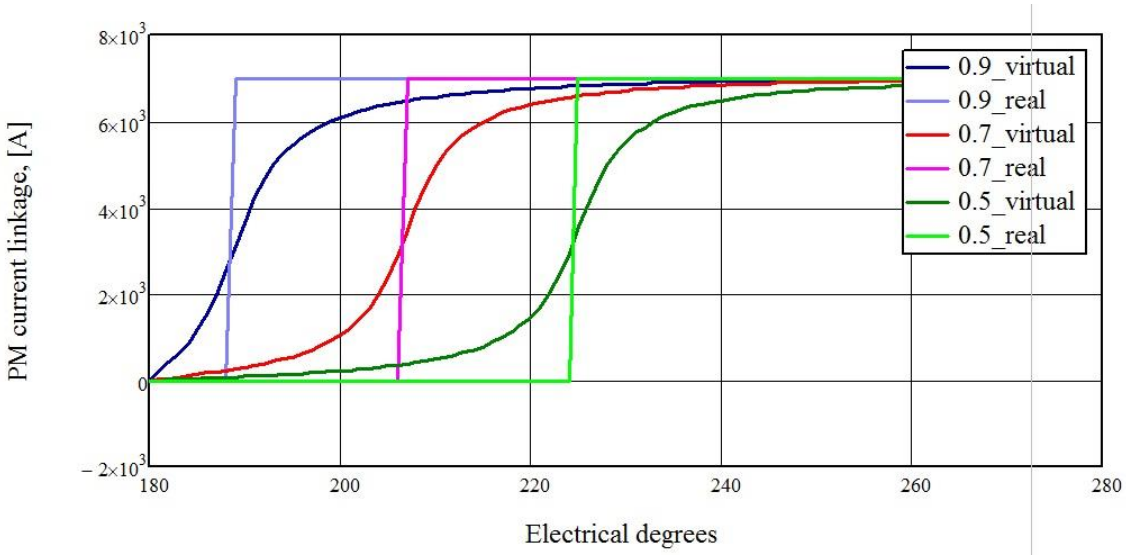

Fig. 21 Comparison of PM current linkages in real case and virtual effective case calculated with the proposed solution for magnets with equal shape, height, location but with different relative PM width α_{pm} = 0.9, 0.7, and 0.5 respectively

3.2.2 Current linkage of the PM when modelling the PM flux density

When the magnetic flux density in the magnet is considered, another formulas of PM current linkage should be used. Generally saying, the air gap flux density cannot be used for accurate analysis of the PM related problems. Air gap flux density, of course, will be very close to the PM flux density, but it will not have the sufficient accuracy at the edges of the magnet. The theory presented in [18] provides quite simple and accurate analytical approach for the PM flux linkage calculation with different magnetization directions. The following equation based on theory in [15] and [20] is used for the description of the PM´s radial component current linkage (the magnetization direction of the PM is radial):

$$\Theta_{\mathrm{PM}}(x) = \sum_{\xi=1,3,5\ldots}\left[\frac{4H_c h_{\mathrm{PM}}}{\xi\pi}\sin\left(\xi\frac{\pi\alpha_{\mathrm{PM}}}{2}\right)\cos\left(\xi\frac{x\pi}{180}+\xi\frac{5\pi}{2}\right)\right]. \qquad (48)$$

The equations for the determination of the PM´s current linkage in case of parallel or Halbach magnetization direction are, in principle, described in paper [20]. These equations are not presented in this paper because the most of the PM machines has radial magnetization direction and the correctness of the equations was not verified by the

authors in paper [20]. The models which will be used in this thesis for verification of the proposed model have radial direction of the magnetization.

3.2.3 Stator current linkage in *d*-axis in normal operation mode

Fig. 21 shows that φ_s is the angle between the stator voltage space vector and the stator current space vector. Usually this angle is used for determination of the power factor of the machine. δ_s is the angle between the PM flux space vector and the stator flux linkage vector, and δ_s is also the angle between the stator voltage space vector and *q*-axis of the rotor reference frame. The PMSM in Fig. 21 can be considered as underexcited machine because stator current space vector $\boldsymbol{i}_s$ is lagging from stator voltage space vector $\boldsymbol{u}_s$. According to the space vector theory *d*-axis stator current linkage can be calculated as following:

$$\Theta_d(x) = \sin(\delta_s - \varphi_s) \sum_\nu \Theta(\nu, x), \tag{49}$$

where $\Theta(\nu, x)$ is determined with Eqs. (8) and (10) from Chapter 4 and ν is the stator winding current linkage harmonics number according to Table 2, x is coordinate in electrical degrees. It is very important to mention that Eq. (49) represents *d*-axis current linkage only at a certain moment of time. The real waveform of the stator current linkage is changing all the time because of harmonics which propagate with speeds different from the speed of the fundamental. Fig. 22 depicts the *d*-axis current linkage of the stator winding at the certain moment of time. The parameters of the winding are following: $m = 3$, $p = 1$, $N = 8$, $I_s = 245$ A, $Q = 24$, $W_{\tau p} = 4/6$, $\delta_s = 24$ deg, $\varphi_s = 18$ deg.

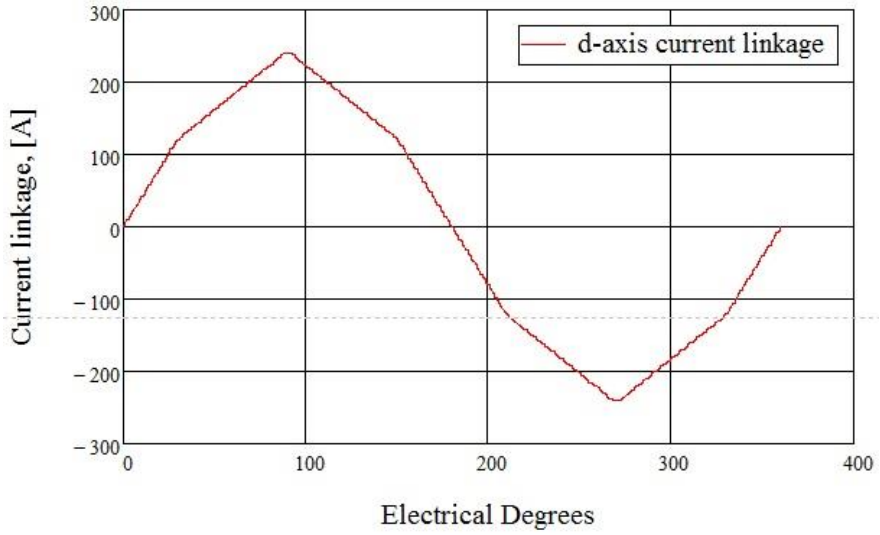

Fig. 22 *d*-axis current linkage of the stator winding at certain moment of the time ignoring the slotting effect. The parameters of the winding are following: m = 3, p = 1, N = 8, I_s = 245 A, Q = 24, W_{tp} = 4/6, δ_s = 24 deg, φ_s = 18 deg.

The detailed analysis of the Fig. 22 should be provided. Theory presented by Pyrhönen *et al.* [2] allows to make the conclusion that the current linkage waveform can be determined as result of the linear current density integration. This means that current linkage of the stator winding have to be the stepped curve because of the slots in the stator. Results from Fig. 22 show that Eqs. 7, 8, 9, 49 taken from [2] cannot be used for accurate determination of the real current linkage of the AC armature winding. However, in the proposed solution the following assumption is made: ignoring the steps of the stator current linkage waveform make very little inaccuracy in the final flux density distribution. Usually, in normal operational mode the current linkage caused by the armature winding does not exceed the current linkage of the PM. This means that PM is the main source of the flux in the air gap of the PMSM. This assumption also significantly decrease accuracy of the model in analysis of the PMSMs with extremely high armature reaction or in case of transients with high values of the currents in the stator winding. This is true also in case of *q*-axis stator current linkage which is described further.

3.2.4 Stator current linkage in *q*-axis in normal operation mode

The same principle as in case of *d*-axis current linkage is applied to *q*-axis current linkage of the stator winding. From Fig. 21 and Eq. (49) *q*-axis current linkage of the stator winding can be determined as following:

$$\Theta_{\mathrm{q}}(x) = -\cos(\delta_{\mathrm{s}} - \varphi_{\mathrm{s}}) \sum_{\nu} \Theta(\nu, x). \tag{50}$$

All variables in Eq. (50) are the same as in case of Eq. (49). The minus sign is used for determination of the rotation direction of the machine. If the rotation direction is counter-clockwise then minus sign has to be used.

Fig. 23 depicts *q*-axis current linkage of the stator winding at certain moment of the time. The parameters of the winding are the same as in case of *d*-axis current linkage: m = 3, p = 1, N = 8, I_{s} = 245 Amp, Q = 24, $W_{\tau\mathrm{p}}$ = 4/6, δ_{s} = 24 deg, φ_{s} = 18 deg.

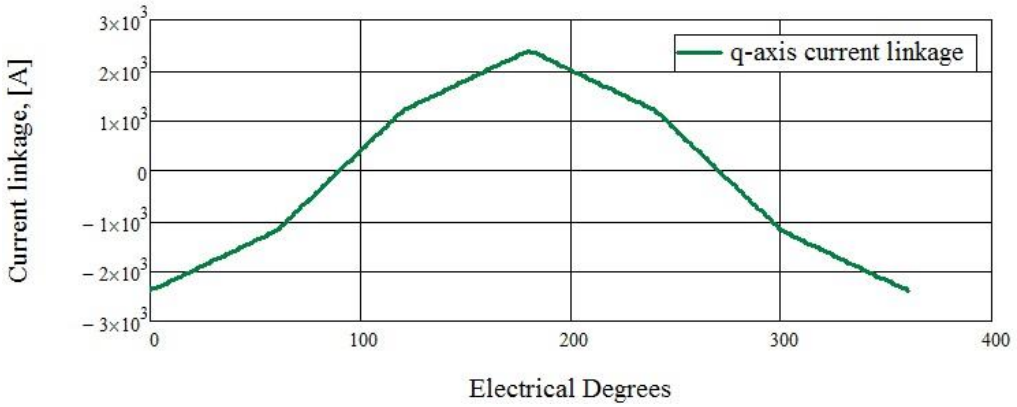

Fig. 23 *q*- axis current linkage of the stator winding at certain moment of the time. The parameters of the winding are the same as in case of *d*- axis current linkage: m = 3, p = 1, N = 8, I_{s} = 245 Amp, Q = 24, $W_{\tau\mathrm{p}}$ = 4/6, δ_{s} = 24 deg, φ_{s} = 18 deg.

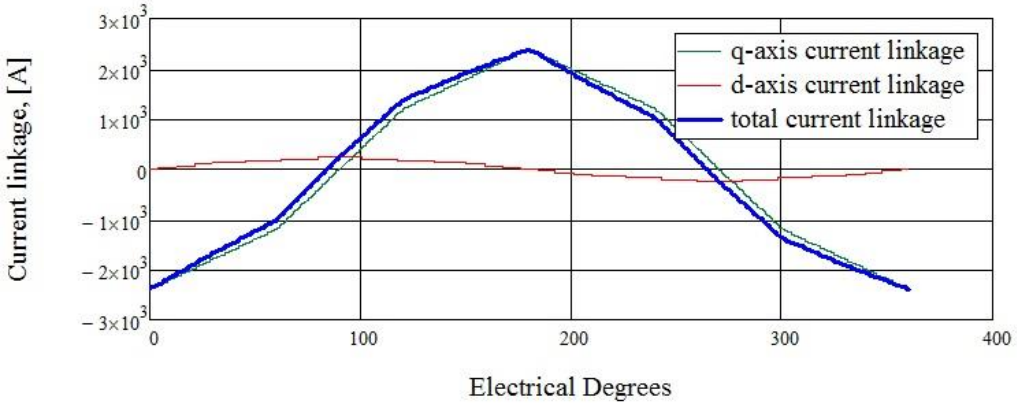

Fig. 24 depicts *q*- and *d*- axis current linkages of the stator winding and total current linkage of the stator winding.

Fig. 24 *q*- and *d*- axis current linkages of the stator winding and total current linkage of the stator winding

From Fig. 24 it can be concluded that the implemented method corresponds well with the theory presented in [2] and [13]. The *d*-axis current has much lower value than *q*- axis

current, and slightly stress the PMSM in demagnetizing direction. This situation is typical for PMSM [13]. It also should be mentioned that this distribution of the stator current linkage corresponds only to a certain moment of the time, but this is enough for the implementation of the proposed solution. In practice, the form of the current linkage is changing simultaneously due to the harmonics. A good approach for the current linkage function that takes into account the dependence on time can be found in [18] and [14].

3.2.5 Current linkage in *d*-axis in case of three-phase short circuit

Current linkage waveform in case of three-phase SSC is determined in the same way as the *d*-axis current linkage in normal operational mode according to Eq. (49). The only difference is that in case of SSC the stator current magnitude is calculated according to Eq. (42) and applied along the *d*-axis so the $\sin(\delta_s - \varphi_s)$ componentin Eq. (49) is equal to 1.

The moment of time in which the stator flux linkage space vector is directed exactly opposite to the PM flux space vector is considered as the worst case of the SSC. At this moment it is assumed that *q*-axis current linkage created by the armature winding is zero. This assumption corresponds well with the theory presented in the first chapter.

3.3 Modelling of the magnetic resistances

Modelling of the magnetic resistances is provided according to a common theory of magnetic circuit discussed in [2], [14], [18]. According to this theory the following equation can be used for the magnetic resistance determination:

$$R_{\mathrm{mi}} = \frac{l}{\mu_0 \mu S}, \tag{51}$$

where R_{mi} is the magnetic resistance of the part of the magnetic circuit with length l, cross-sectional area S and material permeability μ. In case of the proposed model l is width of the "layer" described above. The material permeability in Eq. (51) is equal to the material permeability of the corresponding layer of the model. Special explanation regarding area S should be provided. The proposed solution is calculating magnetic flux density field distribution over two poles (360 electrical degrees). If the PMSM have more than 2 poles the proposed solution automatically takes it into account and makes respective corrections. As the result the proposed model shows the magnetic flux density distribution over 2 two adjacent poles of the PMSM. The length of the machine does not affect the

final result because in the model it is considered that PM and the stator winding create the same value of the current linkage along with the whole length of the machine. According to this assumption S = 1. It should be also mentioned that properties of the material are assumed to be the linear and no saturation of iron occurs. This is fairly true if the machine is correctly designed [2]. Basically it means that all the iron parts of the PMSM magnetic circuit work on the linear part of the *BH*-curve.

3.3.1 Iron magnetic resistance

This magnetic resistance corresponds to the 4th layer of the model presented in Fig. 18. The modelling of the iron magnetic resistance is provided with coefficient *k*. The total current linkage created by the PM and the stator winding is multiplied by the coefficient *k*. The general expression for *k* is the following:

$$k = 1 - \frac{sum\ of\ the\ magnetic\ voltages\ of\ the\ stator\ and\ rotor\ yokes}{total\ magnetic\ voltage}. \quad (52)$$

This data is always determined during the design process to avoid saturation of the magnetic circuit. If data about the magnetic voltages of the machine is absent then *k* can be selected 0.95-0.97 according to the theory provided by Pyrhönen *et al.* in [2].

3.3.2 Air magnetic resistance

This is the second "layer" from the proposed model. The air magnetic resistance with unit cross-sectional surface (S = 1) is determined by the following equation based on Eq. (51):

$$R_{\mathrm{air}}(x) = \frac{\delta}{\mu_0}, \quad (53)$$

where x is the coordinate over two poles of PMSM. Eq. (53) shows that magnetic resistance of the air depends only on physical length of the air gap δ and does not depend on x coordinate.

3.3.3 PM magnetic resistance

Next, the third "layer" in Fig. 18 is observed. It consists of the rotor-surface PM and air (in the space with no PM magnet material). In the proposed model this "layer" is described by the following function:

$$R_{\mathrm{PM}}(x) = \begin{cases} \left[\frac{h_{\mathrm{PM}}}{\mu_0 \mu_{\mathrm{r}}}\right] & if\ 90(1-\alpha_{\mathrm{PM}}) \le x \le 90(1+\alpha_{\mathrm{PM}}) \\ \left[\frac{h_{\mathrm{PM}}}{\mu_0 \mu_{\mathrm{r}}}\right] & if\ 270-90\alpha_{\mathrm{PM}} \le x \le 270+90\alpha_{\mathrm{PM}} \\ \left[\frac{h_{\mathrm{PM}}}{\mu_0}\right] & otherwise \end{cases} . \quad (54)$$

Eq. (54) shows that the third "layer" consists of two linear magnetic resistances: resistance of the magnet and the resistance of the air. Eq. (54) is just one way for the implementation of such kind of approach. Good and quite accurate mathematical representation of this layer can be made by representing the PM and air magnetic resistances by two separate Fourier series. For example, Fig. 25 represents the resulting magnetic resistances of the third "layer" for the different relative widths of the PMs. The parameters of the magnet in all cases are the following: h_{PM} = 5 mm and μ_{r} = 1.05.

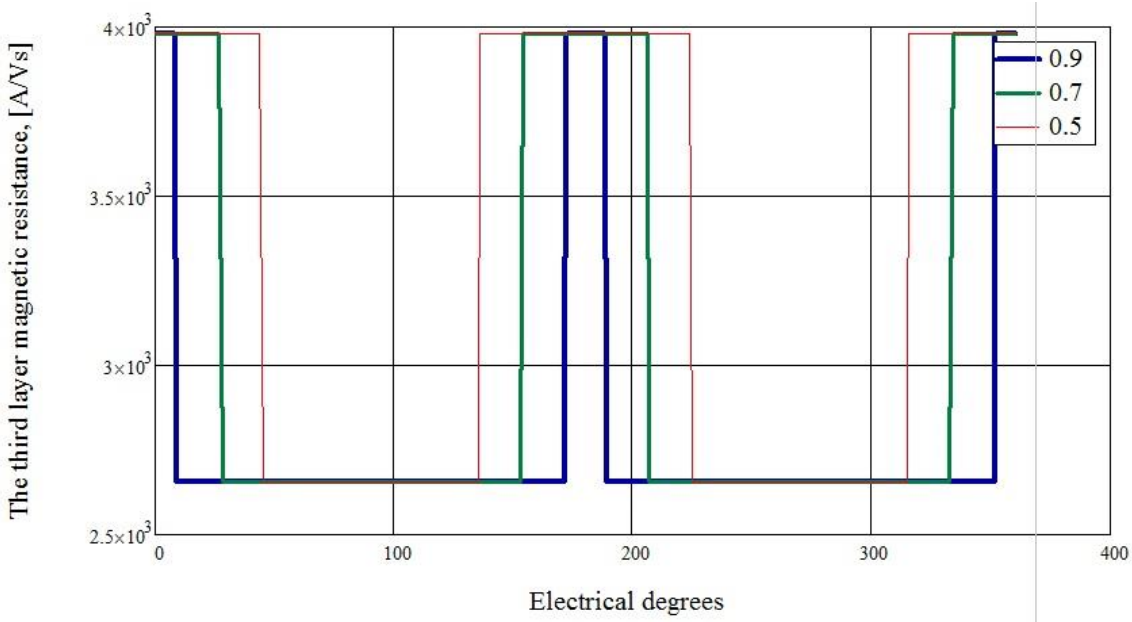

Fig. 25 Resulting magnetic resistances of the third "layer" for the relative widths of the PMs α_{PM} = 0.9, 0.7, and 0.5 respectively, h_{PM} = 5 mm and μ_{r} = 1.05 in all cases.

Fig. 25 shows that Eq. (54) is correct. Analysis of the literature [2] and [1] shows that the relative permeability of the magnet is slightly higher than relative permeability of the air (the difference can be about 4%). That means that the PM magnetic resistance calculated according to Eq. 50 will be lower than the magnetic resistance of the air. Data from Fig. 25 also corresponds well with Eq. (50): the magnetic resistance of the PM is lower than that of air (if all other parameters are the same) because of $\mu_{\mathrm{r}} \ge 1$.

3.3.4 Slot and slot opening magnetic resistance

This magnetic resistance corresponds to the first "layer" of the proposed solution. Analysis of the literature [2], [13], [18], [16] shows that phenomena of the slot opening cannot be ignored during the magnetic flux density prediction. According to the data presented in [2], the slot opening causes a significant decrease of the resulting flux density even they are equipped with semimagnetic wedges. Analysis of the literature [2] shows the phenomenon of the resulting flux density increasing after the slot opening. This phenomenon takes place because of small current which flows in the slot [2]. Data from Pyrhönen *et al.* [2] allows to assume that the slot opening magnetic resistance can be modelled as parabola. It should also be mentioned that effect of slot opening should be modelled in electrical degrees and should take into account pole pair number. In case if pole pair number more than one the number of slots crossing each PM should be divided by p.

For implementing of the slot modelling, first the function which describes one tooth and one slot opening should be presented. The basic function for tooth and slot opening modelling is following:

$$slot(x) = \begin{cases} \left[\frac{180p\left(\frac{\pi D_s}{Q}-b_d\right)}{\pi D_s}\right]^{-2}(h_1+h_2)x^2 \; if \; 0 \le x \le \frac{180p\left(\frac{\pi D_s}{Q}-b_d\right)}{\pi D_s} \\ (h_1+h_2) \; if \; \frac{180p\left(\frac{\pi D_s}{Q}-b_d\right)}{\pi D_s} \le x \le \frac{180p\left(\frac{\pi D_s}{Q}+b_d\right)}{\pi D_s} \\ \left[\frac{180p\left(-\frac{\pi D_s}{Q}+b_d\right)}{\pi D_s}\right]^{-2}(h_1+h_2)\left(x-360\frac{p}{Q}\right)^2 \; if \; \frac{180p\left(\frac{\pi D_s}{Q}+b_d\right)}{\pi D_s} \le x \le 360\frac{p}{Q} \end{cases} . \quad (55)$$

Geometrical parameters for Eq. (55) are determined according to Fig. 19, b_d is tooth width of the machine. The explanation of the parameters used in Eq. (55) is based on the behaviour of the magnetic flux density at the slot opening. The data provided by Pyrhönen *et al.* in [2] allows to make an assumption that the magnetic flux density at the slot opening resembles the parabola. This phenomenon can be modelled by the respective application of the magnetic resistances in this "layer". It is assumed that, where there is no iron, all the space of the first "layer" consists of air or the semi magnetic wedge material. The

height of the first "layer" is determined, obliviously, by parameters presented in Fig. 19. Fig. 26 demonstrates the assumptions which were accepted in modelling this part of the magnetic circuit. In the model it is considered, that the magnetic resistance of the first "layer" is equal to the resistance of the air part of the magnetic circuit in this "layer" with height equal ($h_1 + h_2$) – height depicted by the blue line in Fig. 26.

Fig. 26 depicts one stator tooth and slot opening of the machine and the function which will be used for the analytical model further. The parameters of the machine were selected randomly: $Q = 24$, $b_1 = 1$ mm, $b_d = 6$ mm, $D_s = 100$ mm, $p = 2$, $h_1 = 1$ mm, $h_2 = 3$ mm.

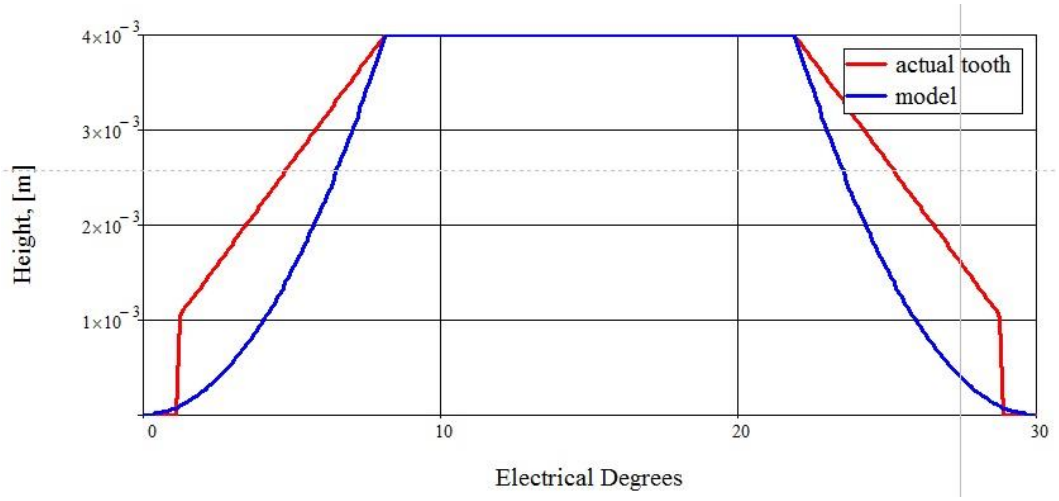

Fig. 26 One stator tooth and slot opening of the machine and the function which will be used for analytical model. The parameters of the machine are selected randomly and described above

Fig. 26 was built according the Eq. (55). It shows that Eq. (55) build the model for first "layer" description and this model takes into account pole pair variations, slot dimensions variations, geometric parameters variation and provide good approach for slot description in electrical degrees.

Next, Eq. (55) should be represented as Fourier series and applied to the proposed model.

The following equations based on theory adopted from [21] are used to represent Eq. (55) in Fourier series:

$$A_1(x) = a_0 + \sum_{n=1}^{\infty}\left[a_n(n,x)\cos\left(nx\frac{2\pi Q}{360p}\right)\right], \quad (56)$$

where

$$a_0 = \frac{Q}{360p}\int_0^{\frac{360p}{Q}} slot(x)dx, \tag{57}$$

$$a_n(x) = \frac{2Q}{360p}\int_0^{\frac{360p}{Q}} slot(x)\cos(nx\frac{2\pi Q}{360p})dx. \tag{58}$$

Generally, the function *slot(x)* can be presented in Fourier series with providing necessary calculation and this can help to avoid Eq. (55), Eq. (57) and Eq.(58) in the proposed model.

Fig. 27 depicts comparison of the model which was build according to Eq. (55) and with using the Fourier series based on Eqs. (56-58). All parameters are the same as in Fig. 26.

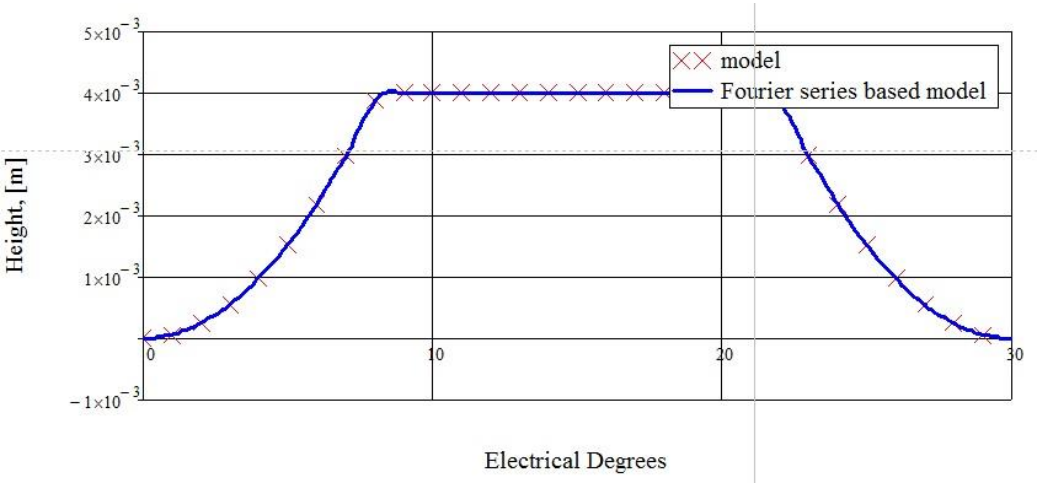

Fig. 27 Comparison of the model which was build according to Eq. 55 and with using the Fourier series based on Eq. (56-58)

Fig. 27 shows that the Fourier transform was correctly applied. Now, according to Eq. (56) the function $A_1(x)$ represents the first "layer" modelling over 360 electrical degrees which corresponds to 2 poles of the machine. If the relative permeability of the iron is assumed to be infinity the following equation describes the first "layer" magnetic resistance:

$$R_s(x) = \frac{h_1+h_2-A_1(x)}{\mu_0\mu_r}, \tag{59}$$

where μ_r is relative magnetic permeability of a wedge material. If slots of the machine are without wedges than $\mu_r = 1$. Fig. 28 depicts the resulting first "layer" magnetic resistance. All parameters are the same as in case of Fig. 26 and Fig. 27, magnetic permeability of the wedge material $\mu_r = 3$.

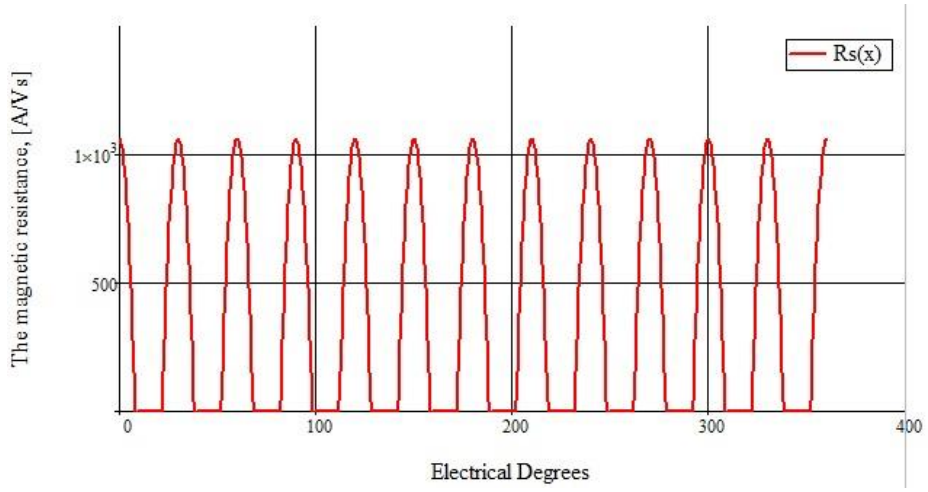

Fig. 27 The first "layer" model that was build according to the chosen parameters

Fig. 27 show that the model takes into account pole pair, number of slots variations. In this case Q = 24 and p = 2, which results to Q/p = 24/2 = 12 slots per 360 electrical degrees. From Eq. (59) it is clearly seen that this model takes into account also the tooth height and magnetic permeability of wedge material possible changing.

3.4 General solution

Now, the general solution should be presented. The following equation based on the observing of the magnetic circuit theory presented in [2], [13], [18] can be presented:

$$B(x) = \frac{\sum \Theta_{\mathrm{i}}(x)}{S(x)(\sum R_{\mathrm{i}}(x))}. \tag{60}$$

Eq. (60) gives the distribution of the magnetic flux density which is changing with x coordinate. In practice Eq. (60) means that the magnetic circuit is divided to a big number of simple linear magnetic circuits and each of the circuit is calculated separately.

Summarizing the above assumptions and observations, especially, Eq. (47), (49), (50), (52), (53), (54), (59), (60) the following equation is used as the general solution for magnetic flux density distribution in the surface mounted PMSM in normal operation mode:

$$B(x) = \frac{k\left(\Theta_{\mathrm{PM}}(x)+\Theta_{\mathrm{d}}(x)+\Theta_{\mathrm{q}}(x)\right)}{R_{\mathrm{s}}(x)+R_{\mathrm{PM}}(x)+R_{\mathrm{air}}(x)}. \tag{61}$$

The accuracy of this model will be investigated in the next chapter.

4 VERIFICATION OF THE THEORY

The verification of the proposed solution is based on the comparison of the resulting magnetic flux density distribution obtained with the proposed model and the results from the FEM simulation of the same rotor-surface-magnet PMSM.

The two operational modes is observed for comparison. In the first mode the PMSM is rotating with nominal torque, speed, current and power factor. All values in this mode are known. The evaluation of the results in this mode is provided with the comparison of the magnetic flux densities in the air gap of the machine and in the outer part of the PM.

The second operational mode is provided by simulation of a three-phase SSC at the terminals of the PMSM. The PMSM is rotating with the same parameters of the normal mode as in the first mode. At some moment of time the terminals of the machine are shorted and the magnetic flux density distribution at the worst time from the magnets' point of view is obtained. The technical data of the PMSM which is used for comparison can be found in Appendix A.

4.1 Normal operational mode

4.1.1 Air gap magnetic flux density

The comparison of the air gap magnetic flux density of the rotor-surface magnet PMSM is presented in Fig. 28. The measurement of the magnetic flux density in FEM program was made at the middle of the air gap. The parameters of the PMSM are listed in Appendix A. The current linkage of the PM in the proposed model was calculated with Eq. (47). The fact that the air gap current linkage of the PM is differs from PM current linkage in PM itself was described in the previous chapter.

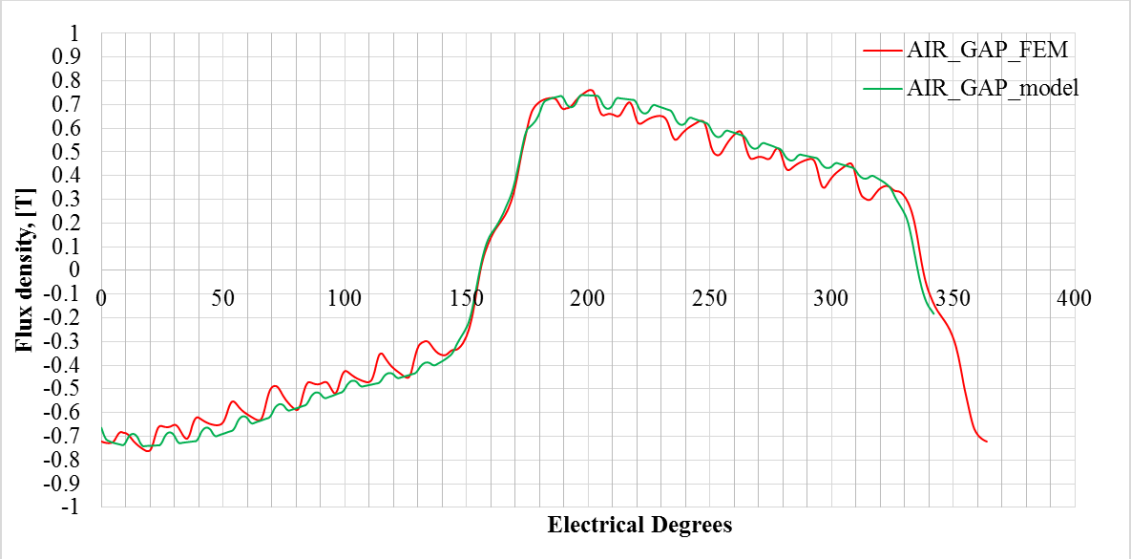

Fig. 28 Comparison of the magnetic flux density in the air gap of the PMSM obtained with FEM program and with the proposed model. AIR_GAP_FEM is the curve which depicts the results obtained from the FEM program, AIR_GAP_model curve represent data obtained with proposed model.

It should be mentioned that the normal magnetic flux density component comparison is presented in Fig. 28. Detailed observation shows that the forms of curves presented in Fig. 28 look very similar. The observation of the curve obtained with the proposed model shows some inaccuracy in the parts of the PM where the magnetic flux density is decreasing due to the slot opening. This allows to make a conclusion that model for the first "layer" which is used to take into account slots and slot openings of the PMSMs should be improved. However, this way of slot modelling is very nicely performing its function in the description of slots and slots opening which are the function of the parameters *p*, *m* and *q*. Generally saying, the function which is used for the slot and slot opening description can be excluded from Eq. (61), because the slot opening has no significant effect on the edges of the PMs which are the most needed points for the analysis.

The most interesting point for the comparison is the edges of the PM. The comparison presented in Fig. 28 shows that the curves are fitting a lot, but still an inaccuracy of the proposed model have to be estimated. For the estimation of the inaccuracy of the proposed solution the one magnet of the PMSM is presented in Fig. 29. The values of the magnetic flux density normal components at the edges of the PM are depicted, too.

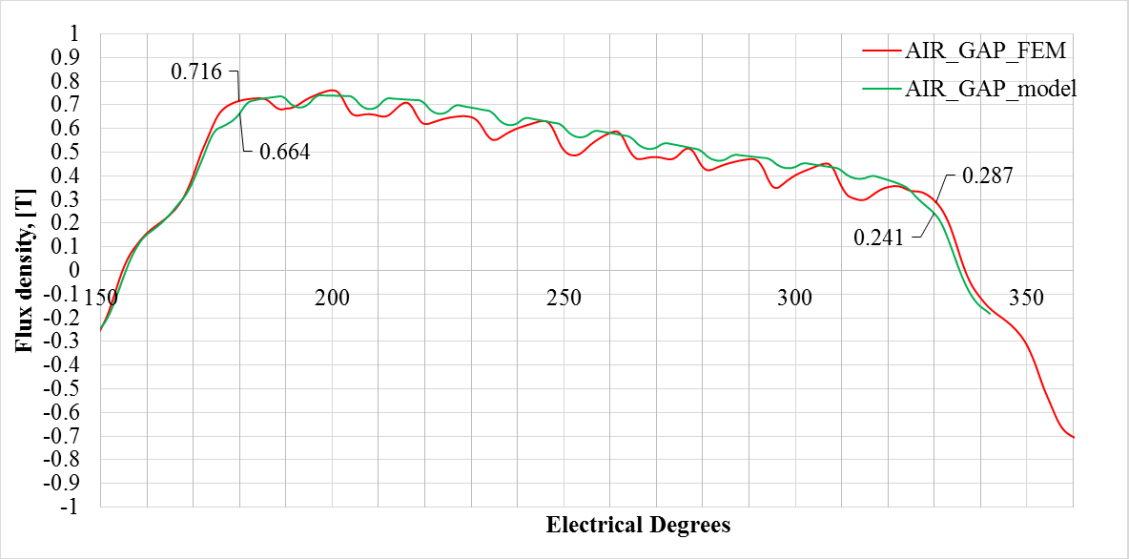

Fig. 29 Magnetic flux density normal component in the air gap over one PM (180 electrical degrees). AIR_GAP_FEM is the curve which is depicts results obtained from FEM program, AIR_GAP_model curve represent data obtained with proposed model.

The magnetic flux densities, determined with the FEM program and with the proposed model in the air gap of the PMSM, are very close to each other. The following formula is used for evaluating the inaccuracy at a certain point of the proposed model:

$$inaccuracy = \frac{(value\ from\ FEM\ program - value\ from\ model\ calculations)}{value\ from\ FEM\ programm} 100\%. \quad (62)$$

The inaccuracy at the leftmost edge of the magnet according to the Eq. (62) is 7.3 %. The rightmost edge of the magnet inaccuracy is 16.4 %. The inaccuracy of the rightmost edge of the PM is obviously high, but it should be mentioned that this part of PM cannot be prone to hysteresis losses.

The theory presented in Chapter 1 states that hysteresis losses can take place if the part of PM experiences field strength variations which change sign of the magnetic field strength in the PM. In other words, flux density of the PM should be very close or even higher of the remanence flux density. Even with inaccuracy of about 20% the rightmost part of the PM is still very far from the remanent flux density.

The leftmost part of the PM is the part of the PM which has the highest probability of the hysteresis losses appearance. The inaccuracy which is less than 10 % is quite a good result for such a simple model but it needs to make the observation of the same model with neglecting of the stator slotting effect. This need can be basically explained by the fact

that the observation of the curve obtained from the model and depicted in Fig. 29 shows the fact of slot affecting at the edge of the magnet. The model should be validated again by neglecting the slot opening effect. The results obtained from the same model by neglecting the stator slotting effect are depicted in Fig. 30. Comparison is made with the same data from FEM as used in Fig. 29.

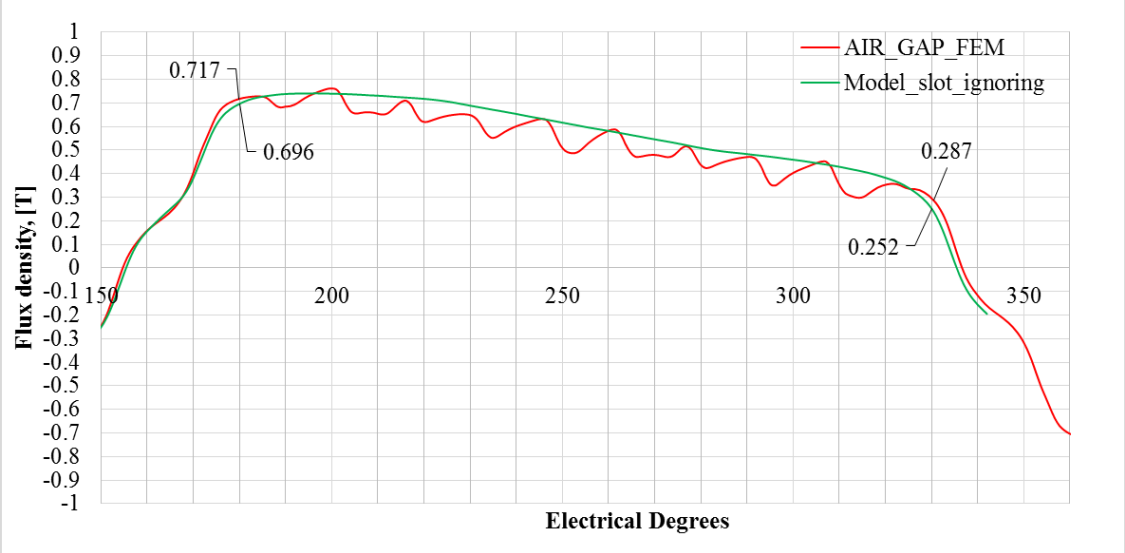

Fig. 30 Comparison the magnetic flux density normal components obtained with FEM program and calculating with proposed model. Now the proposed model is ignoring the stator slotting.

Observation of the same part (leftmost and rightmost) of the PM shows the better results if the stator slotting is ignored. The inaccuracies of the proposed model at the rightmost and the leftmost edge of the PM are now 12.2 % and 2.9 % respectively. As it was previously stated the rightmost edge of the magnet does not represent the practical interest when the designer want to evaluate the possibility of the hysteresis losses in the PMSM. The inaccuracy of the leftmost part of the magnet seems to be sufficient for evaluating the possibility of the hysteresis losses during the design process. It also should be mentioned that the accuracy of the model can be increased with the right determination of the coefficients in Eq. (47). However, from comparison presented in Fig. 30 it is clearly seen that magnetic flux density of the PM parts which have the highest probability of the appearance of the hysteresis losses can be evaluated with inaccuracy less than 5% even with the present coefficients.

4.1.2 Flux density inside the PM

The magnetic flux density normal component inside the PM has the most importance during the analysis the possible problems in the PM. The proposed model allows to calculate the distribution of the magnetic field. The PMs of the PMSM under consideration have radial direction of the magnetization. When applying the proposed model the general solution is used with 2 modifications. The first modification, as was previously stated, is application of Eq. (49) instead of Eq. (48) in the calculation of the PM current linkage. Now the current linkage of the PM has a rectangular form. This can be explained by the assumption that the leakage flux in the PM is very small because of the extremely high magnetic field strength inside the PM. The second assumption is the neglecting of the stator slotting effect in the Eq. (61). The analysis of the FEM results shows little influence the stator slot openings on the resulting magnetic flux density of the PM. This fact is also explained by the very high field strength inside the PM. Summarizing the above information the proposed solution uses the same principle for the determining the distribution of the magnetic flux density normal component as in the case of the air gap with only two differences: the PM current linkage is calculated according Eq. (49) instead of Eq. (48) and the stator slotting component is excluded from the final Eq. (61). Fig. 31 shows a comparison of the FEM results and data obtained with the proposed model. The data about the magnetic flux density distribution from FEM program was measured for the outer layer of the PM.

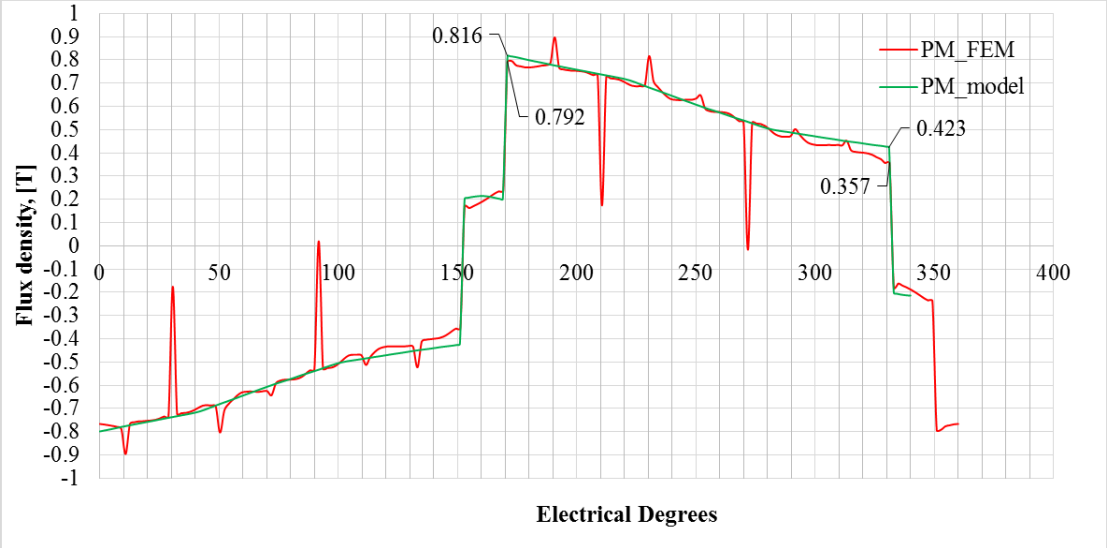

Fig. 31 Comparison of the data obtained from FEM program (PM_FEM) and the magnetic flux density distribution calculated with proposed model (PM_model).

The curves' comparison depicted in Fig. 31 shows a good accuracy of the proposed model. Again, the inaccuracy of the proposed solution at the edges of the PM calculated according to Eq. (62) is 18.5 % for the rightmost part of the magnet and 3% for the leftmost part of the PM.

This part is most important part of this work and detailed explanation of Fig. 31 should be provided. Fig. 32 represents the same data as in Fig. 31 for one pole of the observed PMSM.

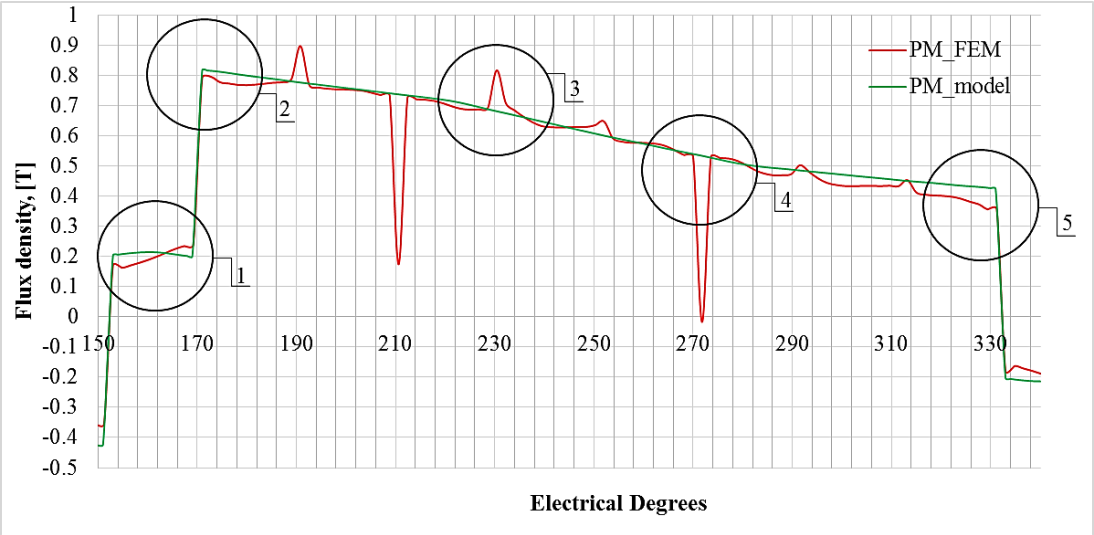

Fig. 32 Data represented in Fig. 31 only for one pole of the PMSM.

The five zones depicted in Fig. 32 should be analysed to verify the proposed model. The first area represents the part of the PMSM`s pole where there is no PM material. In principle, the area does not represent any interest and is verified only to be sure about correct estimation of the armature reaction. This part of the PMSM pole corresponds well with FEM results at least in width of this part of the pole. The differences between the values in this part of the pole can be explained by the neglecting the stator slotting effect in the proposed model. The second area depicted in Fig. 32 is the most important area. The hysteresis losses according to the theory presented in the first chapter have the highest probability of the appearance exactly in this part of the PM because of the highest flux density. It is very important to model this part of the PM with the highest accuracy as possible to be sure the PM magnet flux density is lower that the remanent flux density. Result from analysis of Fig. 30 and Fig. 31 shows ability of the proposed model to evaluate the magnetic flux density at the leftmost part of the magnet with the accuracy less than 5 %. The purpose of the third area is to show the significant peak of the magnetic

flux density at upper layer of the PM. The main reason of such peaks are the aluminium parts between the magnets. The PM over one pole in the FEM observed PMSM is divided into three separate parts. The aluminium material is used between the parts of the PM. The effect of such dividing is clearly seen in Fig. 32 (Area 4). The effect of the PM magnet dividing into separate part is neglected in the proposed solution. The analysis of the Fig. 32 shows that, despite the quite significant effect of the PM division into separate parts on the resulting magnetic flux density, it has no influence on the area most prone to hysteresis losses. The neglecting of the magnet segmentation phenomena in the proposed model has no significant effect on the hysteresis losses analysis. The results from Fig.32 shows that proposed solution can be used in case of the segmented magnet also, without additional decreasing of accuracy in the areas most prone to hysteresis losses. Fig. 33 depicts the half pole of the FEM observed PMSM and the machine which is modelled according to the proposed solution. Literature analysis shows that the correct modelling of PM segmenting is a demanding task.

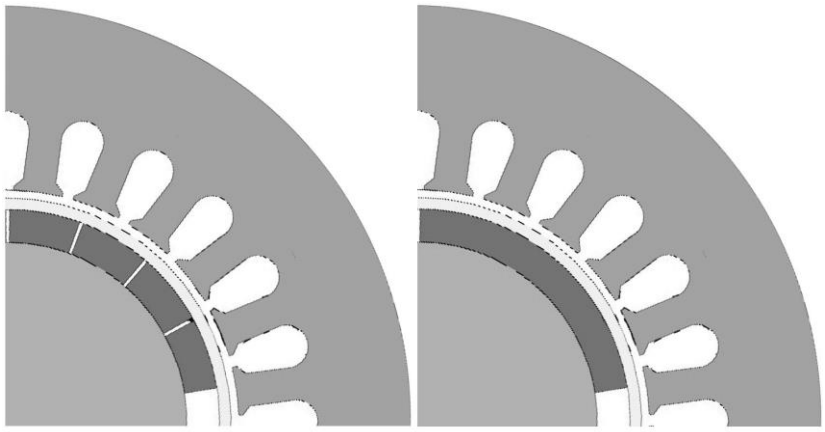

Fig.33 The difference between rotor which is modelled according to the proposed solution and rotor of the FEM observed machine. a) the rotor of FEM observed machine, b) the rotor which is modelled according to the proposed solution. The effect of the PM segmenting can be neglected in the proposed solution without losing the accuracy in case of the hysteresis loss analysis. The Fig. 33 depicts the half pole of the each machine.

The phenomenon of the PM flux density significant reduction is depicted at fourth area in Fig. 32. This phenomenon can be easily explained by the fact of dividing one magnet of the pole by three separate parts in the PMSM under the observation. The reducing of the resulting magnet flux density is caused by absence of the PM material between separate parts of the magnets over one pole. This phenomena does not play significant

role in the estimation of the magnetic flux density at the edges of the magnet. The effect of PM division on some separate parts is neglected in the proposed model. The fifth area shows the rightmost part of the magnet. According to proposed solution, the inaccuracy between FEM program and model results should be small. The data analysis provided in Fig. 30 and Fig. 31 shows the inaccuracy about 20 %. The accuracy of the model in the area 5 can be insufficient for the evaluating of the PM flux density distribution. It also should be mentioned that according to the comparison of the results from proposed model and results from FEM program, the proposed solution at area 5 always calculates the higher values. The most important part which is depicted by the area 2 in Fig. 32, however, have sufficient accuracy for fast magnetic flux density normal component evaluation.

4.1.3 Application of the Carter`s factor theory

Previous observations revealed insufficient accuracy of the stator slots and slots opening modelling. Now, the same model is observed with slot openings modelling according to the Carter`s theory. The part of the Eq. (61) which used for the slot and slot opening magnetic resistance modelling is removed. The physical air gap is corrected with Carter factor according to the following equation:

$$\delta_{\mathrm{es}} = k_{\mathrm{Cs}}\delta\,, \tag{63}$$

where δ_{es} is the equivalent length of the air gap according to the Carter`s theory and k_{Cs} is the Carter factor determining by the following equation:

$$k_{\mathrm{c}} = \frac{\tau_{\mathrm{u}}}{\tau_{\mathrm{u}} - b_1 \frac{\frac{b_1}{\delta}}{5+\frac{b_1}{\delta}}}\,. \tag{64}$$

The observed machine has slotting only at the stator side and that is why Carter factor is determined only for the stator slot opening. The parameter b_1 used for the determination of the width of the slot opening should be divided by the relative permeability of the magnetic wedge material. In this case the magnetic flux density is calculated in the upper layer of the PM according to Eq. (61) with three modifications: stator slot modelling function is excluded from the Eq. (61), the air gap length is corrected with Carter factor and PM current linkage is calculated with Eq. (48). The Carter factor k_{Cs} in case of observed machine is 1.002. The value differs only slightly from 1. This value mainly can

be explained by very good properties of the magnetic wedges material and relatively large air gap of the observed PMSM. The results obtained from this value of Carter factor can be misleading, that is why the new Carter factor should be calculated for the same machine without the magnetic wedges. In case of the non-magnetic wedges in the stator slot openings (all other parameters are the same) the Carter factor will be 1.021. Fig. 34 depicts the data about PM flux density distribution in the upper layer obtained with FEM program and calculating with proposed model for two values of the Carter factor.

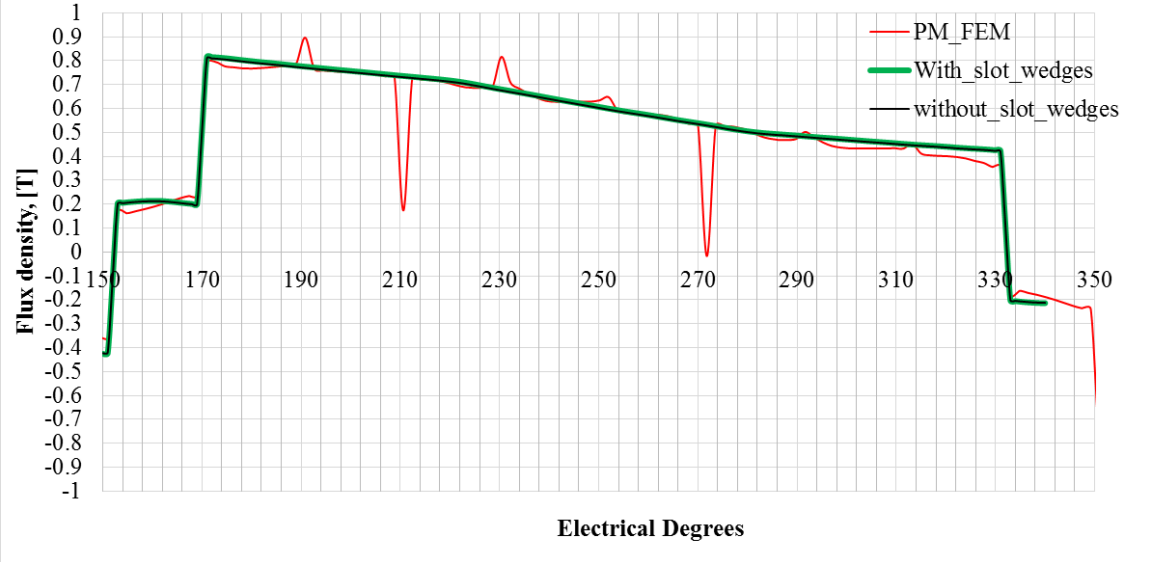

Fig. 34 Comparison of the magnetic flux density distribution obtained from FEM program and calculated with the proposed model. Slot modelling function in the proposed model is replaced according to the Carter factor theory. Curve "With_slot_wedges" takes into account magnetic wedge material in the slots, in the curve "without_slot_wedges" it is assumed that there is no magnetic wedge material in the slots.

The analysis of Fig. 34 shows very close curve fitting. This can be explained by the small dependence of the equivalent air gap from the stator slotting (the worst case according to the analysis is 2.1 %). Obtained results can be easily explained with Eq. (64). In case of the machine which is under observation the physical air gap is relatively large (5 mm). This air gap length results in very small effect of the slot opening on the Carter coefficient. This conclusion corresponds well with the results presented in Fig. 34. Generally saying, the Carter factor theory is used to determine the average value of the magnetic flux density over the slot pitch, but main task of the proposed model is determine instantaneous values over the PM. Moreover, Eq. (64) and analysis of the data presented by Pyrhönen *et al.* in [2] shows that with smaller air gap length the effect of the Carter factor can be significantly higher (up to 20 % or more) and this can reduce the accuracy of the proposed

model a lot. The application of the Carter factor in the proposed model results in poor accuracy.

4.1.4 Assumption that air have permeability of the PM

The accuracy of the proposed model should be observed with assumption that air has the permeability of the PM. The analysis of the literature presented in [2] and [1] revealed that the relative permeability of the PM differs no more than 5% from air (in case of this machine the PM's μ_r is 1.044). This assumption can simplify the proposed model a lot. The following correction were made in the model: all the magnetic resistances are used for the air description are divided by the relative permeability of the PM. It is equivalent to representing the magnetic resistances of the air gap and PM by one resistance of the PM with relative width $\alpha_{PM} = 1.0$ and height $\delta + h_{PM}$. Stator slotting resistance is excluded from the Eq. (61). The comparison of the results obtained with FEM program and according the proposed model with the respective assumptions is depicted in Fig. 35.

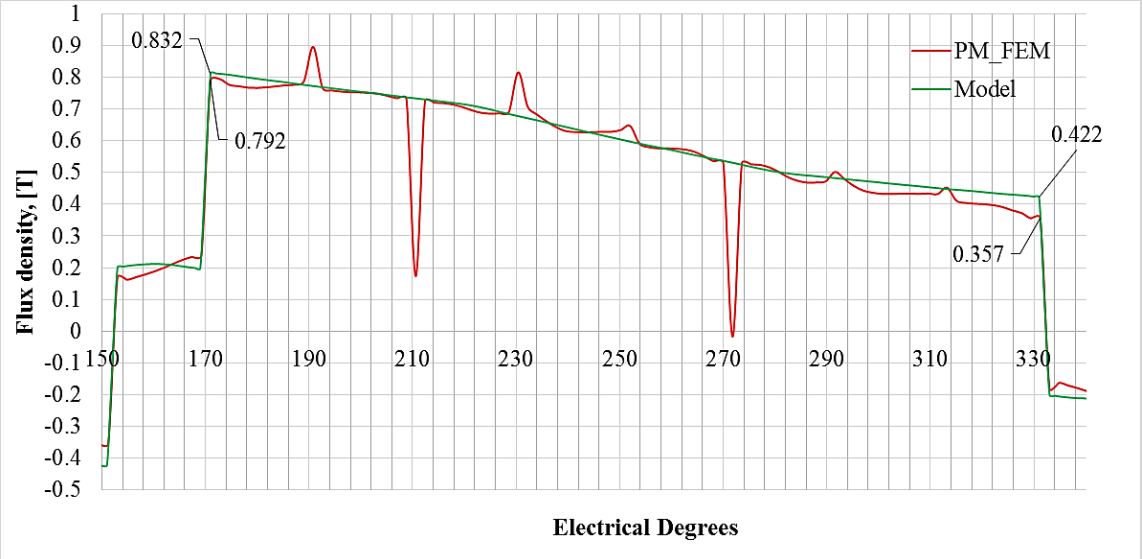

Fig. 35 Comparison of the magnetic flux densities at the edges of the PM. "PM_FEM" curve shows data from FEM program about the magnetic flux density normal component distribution at the upper part of the magnet. "Model" curve shows the magnetic flux density normal component distribution obtained with the proposed model which takes into account the assumptions described in this chapter.

The inaccuracy calculated with Eq. (62) shows now 5.1% and 18.2% at the leftmost and the rightmost parts of the PM respectively. As it was previously stated, it is most important to know the magnetic flux density at the leftmost part of the PM. The accuracy of the proposed model is still enough at least for preliminary design. It should be mentioned also that, in practise, the relative permeability of the PM $\mu_r = 1–1.05$. This fact

results in decreasing of the air magnetic resistance and decreasing the accuracy of the proposed model. However, observations of the model show that in any case the inaccuracy of the proposed model at the leftmost part of the magnet will not exceed 10%.

4.2 Three phase short circuit

The short circuit is very difficult phenomenon for the modelling. The FEM based programs are used for the accurate determination of the magnetic flux density distribution during the short circuit. In this subchapter the comparison is provided between results obtained from FEM program and data calculated according to the proposed model. The worst time t_{max} of the SSC for the PM according to the theory presented in Chapter 1 can be calculated with Eq. (24). The worst time t_{max} for the observed PMSM is 0.00125 s after short circuit took place. The resulting curves are depicted in Fig. 36.

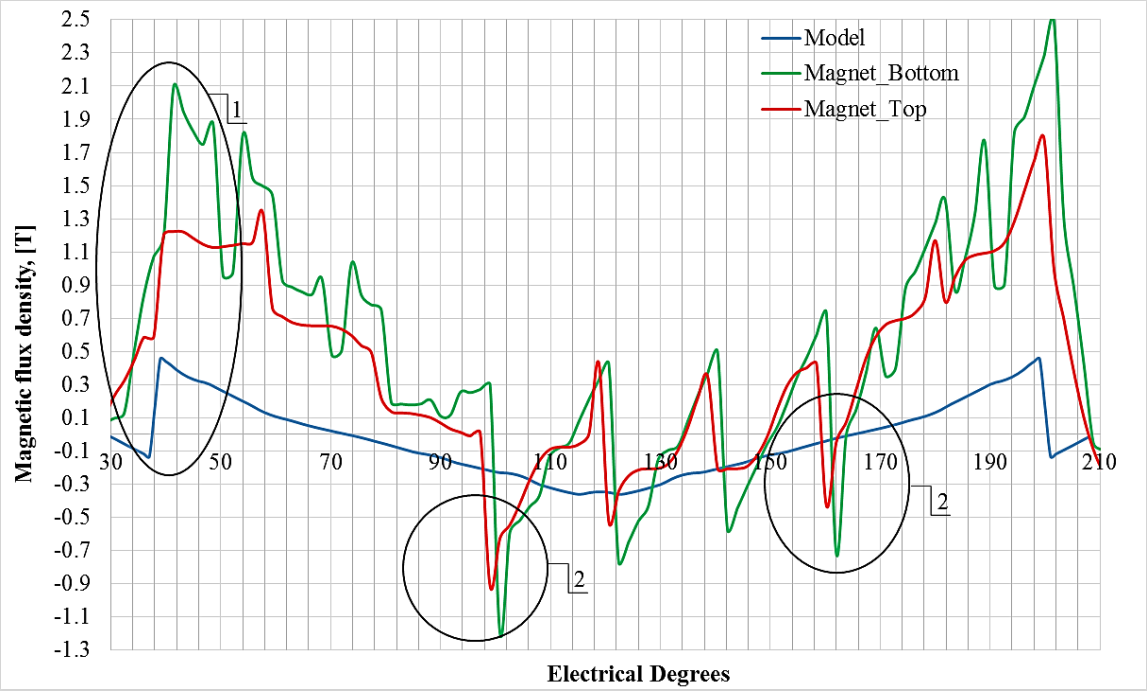

Fig. 36 Comparison of the magnetic flux density normal component distribution over one pole of the PMSM. The "Model" curve is representing the data calculated with the proposed model. "Magnet_bottom" and "Magnet_Top" curves show the magnetic flux density distribution over the same pole according to the data from FEM program for bottom and the top of the PM.

The analysis of Fig. 36 shows that the results obtained with the proposed model differ significantly from the data obtained with FEM program. The bottom of the PM is prone to demagnetization more than the top of the PM. This phenomenon can be explained by the fact that the surface area of the PM at the bottom is smaller than at the top. The

different diameters of the bottom and the top ($0.5(D_r - 2h_{PM})$ and D_r respectively) result in the different magnetic flux densities in the top and in the bottom of the PM. The areas depicted in the Fig. 36 should be analysed. Area 1 shows the magnetic flux density distribution over the left edge of the PM. The data from FEM program in Area 1 in Fig. 36 significantly differs from the model results. However, the theory presented in Chapter 1 allows to conclude that there is no demagnetization phenomenon occurring in this part of the magnet because of high magnetic flux density with positive sign. The areas with number 2 should be excluded from the analysis, too because the extreme decreasing of the flux density was caused by the segmentation of the PM.

The most important part for the comparison is in the middle of the PM, because according to FEM results presented in Fig. 37 the middle part of the PM is most prone to the demagnetization. The theory presented in Chapter 1 states that the middle part is most prone to demagnetization during a three phase short circuit. Fig. 36 depicts the smallest values for the PM flux density in the magnet. The data is the same as in Fig. 37.

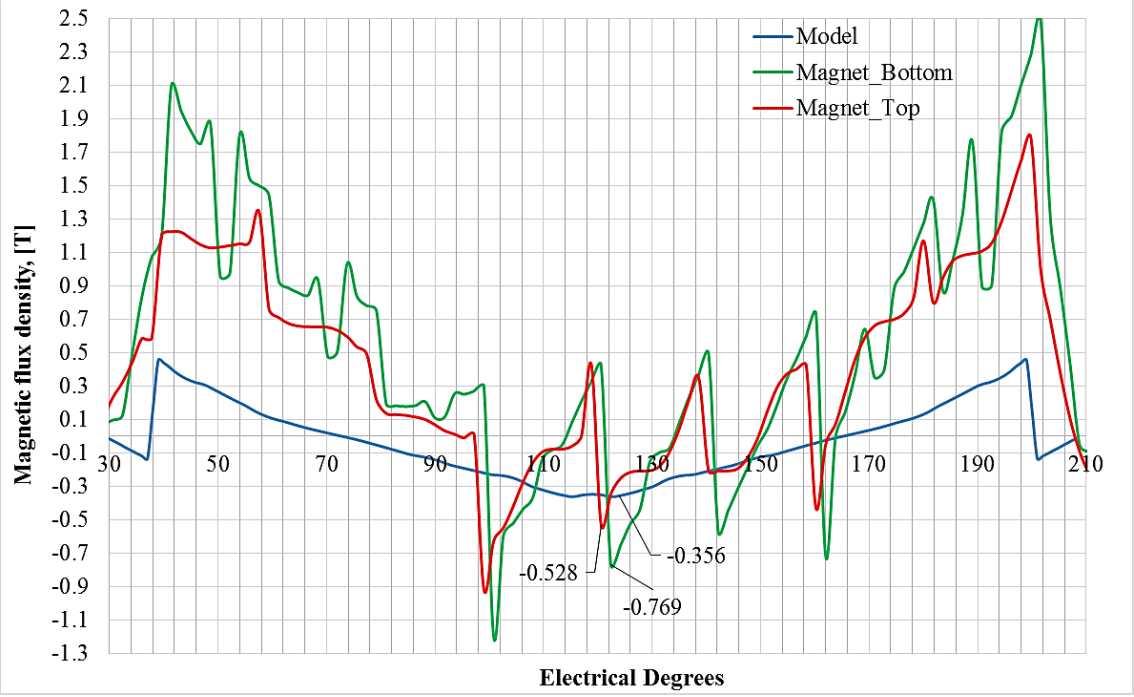

Fig. 37 Comparison of the lowest magnetic flux densities in the middle of the PM. The curves are the same as in Fig. 36

The comparison of the curves presented in Fig. 37 shows fairly good fitting in the form of the curves. The slot opening modelling function, obliviously, was modelled with insufficient accuracy. The inaccuracy of the lowest flux density determining with the

proposed model is 32.6 % and 53.7 % for the top and the bottom of the magnet respectively. The accuracy of the proposed method is obviously insufficient for the magnet flux density analysis during three phase short circuit. It also should be mentioned that the saw-tooth form of the resulting magnetic flux density can be result of the stator armature reaction. During the short circuit due to the extremely high magnitudes of the stator currents the armature winding current linkage cannot be considered as smooth curve. This fact requires the improving of the armature winding current linkage modelling in the proposed model by taking into account the stepping phenomena.

5 CONCLUSION

PMs are widely used in PMSMs due to their good properties. The most common reasons which result in decreasing of the PM properties were analysed in this thesis. These reasons are the hysteresis losses in the PMs in the normal operational mode and the PM demagnetization risk due to a short circuit. The main purpose of this thesis was to create a simple analytical approach which allows to estimate the magnetic flux density at the worst points from PM's point of view in the normal operational mode and in the case of a short circuit. This approach should allow to avoid FEM simulation in the preliminary design.

The theory of the magnetic circuits was used for the analysis of the magnetic flux density in the air gap of the PMSM and in the outer layer of the PM. The current linkage created by the PM was calculated according to the common theory of the magnetic circuit which was used in most papers regarding the PM magnetic flux density analysis when the analysis was provided in the upper level of the PM. However, in case of the air gap flux density analysis a new model for the PM current linkage in the air gap was developed. This model can easily and quite accurately take into account very complicate phenomenon of the PM flux leakage. The coefficients used in the model of the PM current linkage in the air gap can be estimated more accurately to increase the accuracy of the model, but the comparison with the results obtained with FEM based program shows very little difference compared to the results calculated with the proposed model.

An armature reaction model was derived in the thesis. The model is based on theory presented by Pyrhönen *et al.* in [2] and the space vector theory. This model is using the parameters of the winding and the PMSM which were determined during the design process. Analysis of the results shows good fitting of the resulting magnetic flux density obtained with FEM program and with the proposed model. However, the resulting current linkage of the stator winding does not correspond well with theory presented by Pyrhönen *et al.* in [2]. According to the theory the stator current linkage has to be the stepped curve because of the stator slotting. The resulting form of the stator current linkage calculated with the proposed model is smooth. This fact can give poor accuracy in case of the narrow slots in the stator and in the case of extremely high armature reaction. The assumption of neglecting the stator slotting in the stator current linkage model, however, can be

compensated by the extremely high field strength in the PM. The comparison of the curves obtained with FEM program and calculated with the proposed model shows good fitting. As it was previously stated, the armature winding generates a large number of harmonics. These harmonics travel with the speed different from the fundamental harmonic. The proposed model of the stator current linkage allows to obtain the current linkage at the certain moment of the time when all the phase shifts of the harmonics generating by the armature winding are equal to zero. This is, in principle, sufficient for the preliminary design of a PMSM.

The magnetic flux density normal component curves in the middle of the air gap and in the outer layer of the surface mounted PM were obtained for the normal operational mode of the observed PMSM. The comparison between data obtained from FEM program and calculated with the proposed model was provided. The air gap flux density cannot be used for the PM hysteresis loss risk analysis because of the flux leakage effect on the edges of the PM. However, the comparison with FEM results shows that the analytical equation for the PM current linkage description provides quite an accurate way for estimating the magnetic flux density produced by the PM in the air gap. This analytical approach for the PM current linkage can be used in other tasks.

The model accuracy was evaluated in the parts of the PM which are most prone to hysteresis losses. These parts are the edges of the magnet which have the highest flux density. The inaccuracy of the proposed model at the edge of the PM with the highest flux density was less than 5% compared to the results from FEM program. Such a result allows to conclude that the accuracy of the proposed model is sufficient for the preliminary design. The curve of the magnetic flux density calculated with the model corresponds well with the data obtained from FEM program along the whole pole of the machine. However, significant inaccuracy was detected at the part of the PM with the lowest magnetic flux density during the normal operational mode. This fact could be analysed in more details in further work. In this thesis the main task for the model in the normal operational mode is to predict to possibility of the hysteresis losses' appearance. According to the theory presented in the first chapter, these losses can occur only when the magnetic flux density of the PM is close to the remanent flux density of the PM material. The analysis of the FEM results shows that the edge of the PM with the lowest flux density is very far from remanent flux density. This allows to conclude that the

inaccuracy even 20% will be enough to avoid possible hysteresis loss risk during the preliminary design. Most part of the resulting curve calculated with the proposed model fits very well with the curve obtained with using the FEM program.

The analysis of such assumptions as using the Carter factor theory and assuming that the permeability of air is equal to the permeability of PM was provided. Despite the fact that application of the Carter factor resulted in good fitting of the curves, these results can be misleading because the air gap of the PMSM under the observation was large. The smaller air gap will, obviously, result in higher Carter factor and larger equivalent air gap. This will significantly reduce the accuracy of the proposed solution. The application of the Carter factor theory will reduce the accuracy of the model a lot in case of a small air gap. Instead, the analysis of the results obtained when the permeability of air assumed to be equal the permeability of air revealed that the accuracy of the proposed model became slightly lower that in case of precise setting the magnetic resistances of the magnetic circuit in the proposed model. The inaccuracy does not exceed 6% and 20% at the magnet's edge with the highest and lowest flux density respectively. This allows representing PM and air gap of the PMSM as one magnetic resistance with sum height of PM and air gap and permeability of the PM, and still obtain quite precise results comparing with FEM program.

Short circuit is a very chaotic process and still no good analytic approach has been developed for the magnetic flux density distribution during this phenomenon. In this thesis the space vector theory based approach was used for the analysis of a three phase short circuit. The three phase symmetrical short circuit is, probably, the simplest case of the short circuit faults. The results presented in Chapter 4 show that the derived model provided the shape of waveform which is very similar to the results obtained from FEM program. However, neglecting the stator slot openings and saturation of the rotor due to its difficulty result in poor accuracy of the model. The method of the short current calculation has its own inaccuracy, too. Observation of the results from Chapter 4 shows that the inaccuracy for the worst magnet's point calculation is about 50 %. The proposed solution for the SSC needs further development. It also should be mentioned that the proposed method for the calculating of the three phase short circuit current allows very easily to estimate the worst time instant of the short circuit for the PM. For sufficiently

high speeds the worst time of the short circuit can be estimated with only two parameters: rotor electrical speed and the load angle before the time instant when SSC occurs.

FURTHER WORK

Further work can be related to more precise modelling of the current linkage waveform, stator slot resistance and the magnetic flux density distribution during the short circuit. The current linkage waveform should take into account the stator slotting and should be dependent on time.

The stator slot resistance model has to be completely renewed. Probably, it should take into account such phenomenon as increasing the resulting flux after the slot opening. This phenomenon can be neglected during normal operation mode but during the short circuit the correct modelling of the stator slotting is extremely important due to high armature currents.

The three phase short circuit is the simplest case of the short circuit faults but not most damaging case according to the FEM based results observation. The model for three phase SSC should be updated and new approach for the other type of SC faults should be derived.

REFERENCES

[1] Juha Pyrhönen, Sami Ruoho, Janne Nerg, Martti Paju, Sampo Tuominen, Harri Kankaanpää, Raivo Stern, Aldo Boglietti and Nikita Uzhegov. 2014. Hysteresis Losses in Sintered NdFeB Permanent Magnets in Rotating Electrical Machines. IEEE Transactions on Industrial Electronics.

[2] Juha Pyrhönen, Tapani Jokinen and Valeria Hrabovcova. 2014. Design of Rotating Electrical Machines. John Wiley & Sons.

[3] Ruoho S. 2011. Modeling Demagnetization of Sintered NdFeB Magnet Material in Time-Discretized Finite Element Analysis. Doctoral dissertation. Aalto University.

[4] F. Dubas, A. Rahideh.2014. Two-Dimensional Analytical Permanent-Magnet Eddy-Current Loss Calculations in Slotless PMSM Equipped With Surface-Inset Magnets. IEEE Trans. Magn., vol. 50, no. 3, article#: 6300320.

[5] B. Aslan, E. Semail, and J. Legranger. 2014. General Analytical Model of Magnet Average Eddy-Current Volume Losses for Comparison of Multiphase PM Machines With Concentrated Winding. IEEE Trans. Energy Convers, vol. 29, no. 1, pp. 72–83.

[6] A. Fukuma, S. Kanazawa, Daisuke Miyagi, and N. Takahashi. 2005. Investigation of AC Loss of Permanent Magnet of SPM Motor Considering Hysteresis and Eddy-Current Losses. IEEE transactions on magnetics, vol. 41, no. 5.

[7] Xu Tang, Xiuhe Wang. 2014. Calculation of Magnets' Average Operating Point during the Starting Process of Line-start Permanent Magnet Synchronous Motor. 17th International Conference on Electrical Machines and Systems (ICEMS).

[8] Brian A. Welchko, Thomas M. Jahns, Wen L. Soong and James M. Nagashima. 2003. IPM Synchronous Machine Drive Response to Symmetrical and Asymmetrical Short Circuit Faults. IEEE transactions on energy conversion, vol. 18, no. 2.

[9] Ne-Fe-B magnet type 453 A characteristics. Available from http://www.neorem.fi/files/neorem/product-PDF/permanent%20magnets/453a.pdf (accessed 3.3.2015)

[10] G. A. Jubband R. A. McCurrie. 1987. Hysteresis and Magnetic Viscosity in a Nd-Fe-B Permanent Magnet. IEEE transactions on magnetics, vol. mag-23, no. 2.

[11] G. Zhao, L. Tian, Q. Shen, R. Tang. 2010. Demagnetization Analysis of Permanent Magnet Synchronous Machines under Short Circuit Fault. Power and Energy Engineering Conference (APPEEC), 2010 Asia-Pacific.

[12] Michael Meyer, Joachim Böcker. 2006. Transient Peak Currents in Permanent Magnet Synchronous Motors for Symmetrical Short Circuits. SPEEDAM 2006, International Symposium on Power Electronics, Electrical Drives, Automation and Motion Publication series.

[13] Juha Pyrhönen. 2010. Electrical Drives lecture notes. LUT, Department of Electrical Engineering.

[14] G. Dajaku, D. Gerling. 2012. Air-Gap Flux Density Characteristics of Salient Pole Synchronous Permanent-Magnet Machines. IEEE transactions on magnetics, vol. 48, no. 7.

[15] Amuliu Bogdan Proca *et al.* 2003. Analytical Model for Permanent Magnet Motors With Surface Mounted Magnets. IEEE transactions on energy conversion, vol. 18, no. 3.

[16] G. Dajaku, D. Gerling. 2010. Stator Slotting Effect on the Magnetic Field Distribution of Salient Pole Synchronous Permanent-Magnet Machines. IEEE transactions on magnetics, vol. 46, no. 9.

[17] R. Curiac, H. Li. 2011. Improvements in energy efficiency of induction motors by the use of magnetic wedges. Copyright Material IEEE, Paper No. PCIC-2011-42

[18] G. Dajaku, D. Gerling. 2010. Determination of Air-Gap Flux Density due to Magnets using the New Analytical Model. XIX International Conference on Electrical Machines - ICEM 2010, Rome.

[19] Juha Pyrhönen *et al*. 2010. Permanent-Magnet Length Effects in AC Machines. IEEE transactions on magnetics, vol. 46, no. 10

[20] A. Rahideh *et al*. 2012. Analytical Magnetic Field Calculation of Slotted Brushless Permanent-Magnet Machines With Surface Inset Magnets. IEEE transactions on magnetics, Vol. 48, No. 10.

[21] Mohan *et al*. 2003. Power electronics. Converters, Applications and Design. Third edition. John Wiley & Sons.

APPENDIX A Technical parameters of a rotor surface magnet PMSM used in the analysis as example

P, [W]	50000
n, [rpm]	6000
m	3
τ_p, [m]	0.188
Q	24
q	4
p	1
N	8
H_c, [A/m]	820000
B_r, [T]	1.02
D_r, [m]	0.110
α_{PM}	0.9
h_{PM}, [m]	0.0085
δ, [m]	0.005